MASSACHUSETTS INSTITUTE OF TECHNOLOGY

Ocean Engineering

Cambridge, Massachusetts 02139

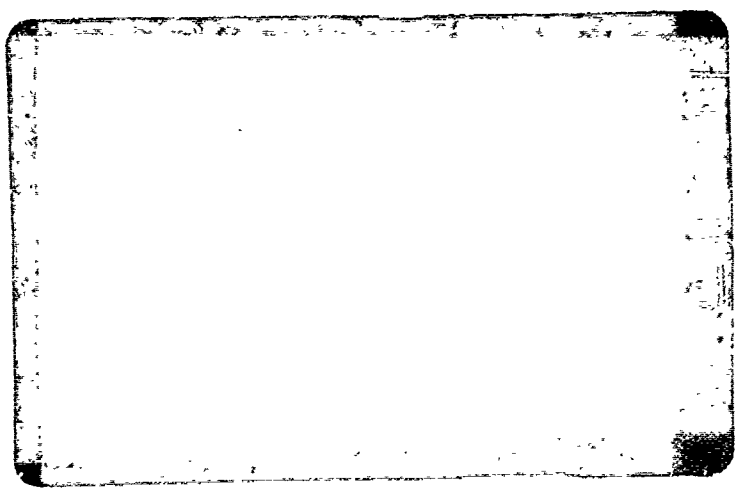

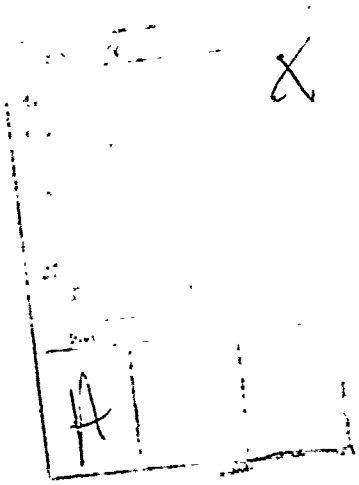

MASSACHUSETTS INSTITUTE OF TECHNOLOGY
Department of Ocean Engineering

Report 75-6

EXPERIMENTAL OPTIMIZATION OF PROPELLER RUDDER ORIENTATION FOR MINIMUM VIBRATORY LOADING

by

Justin E. Kerwin
Anthony B. Zolotas

February 1975

Prepared for
Naval Ship Engineering Center (SEC 6136)
Hyattsvile Md. 20782

This work was supported by the Office of Naval Research, Contract N00014-67-A-0204-0087, M.I.T. OSP 81694.

SECURITY CLASSIFICATION OF THIS PAGE *(When Data Entered)*

REPORT DOCUMENTATION PAGE

READ INSTRUCTIONS BEFORE COMPLETING FORM

1. REPORT NUMBER: (14) 75-6
2. GOVT ACCESSION NO.
3. RECIPIENT'S CATALOG NUMBER

4. TITLE *(and Subtitle)*: (6) "Experimental Optimization of Propeller Rudder Orientation for Minimum Vibratory Loading"
5. TYPE OF REPORT & PERIOD COVERED: (9) Final Report, 71
6. PERFORMING ORG. REPORT NUMBER

7. AUTHOR(s): (10) Justin E. Kerwin, Anthony B. Kolotas
8. CONTRACT OR GRANT NUMBER(s): (15) NEW N00014-67-A-0204-0087

9. PERFORMING ORGANIZATION NAME AND ADDRESS
Department of Ocean Engineering
Massachusetts Institute of Technology
77 Mass., Ave. Cambridge, Ma. 02139

10. PROGRAM ELEMENT, PROJECT, TASK AREA & WORK UNIT NUMBERS

11. CONTROLLING OFFICE NAME AND ADDRESS: (11)
Office of Naval Research

12. REPORT DATE: (12) February 1975
13. NUMBER OF PAGES: 104 (124 p.)

14. MONITORING AGENCY NAME & ADDRESS *(if different from Controlling Office)*

15. SECURITY CLASS. *(of this report)*: Unclassified
15a. DECLASSIFICATION/DOWNGRADING SCHEDULE

16. DISTRIBUTION STATEMENT *(of this Report)*
Distribution of this document is unlimited

17. DISTRIBUTION STATEMENT *(of the abstract entered in Block 20, if different from Report)*

18. SUPPLEMENTARY NOTES

19. KEY WORDS *(Continue on reverse side if necessary and identify by block number)*
Ship Vibration
Propeller Vibration
Rudders
Ship Maneuverability

20. ABSTRACT *(Continue on reverse side if necessary and identify by block number)*
Propeller induced vibratory forces acting on the rudder of a water tunnel simulation of the SEA CONTROL SHIP are measured as a function of longitudinal and transverse clearance in order to determine an optimum location. The influence of propeller-rudder clearance on steady state propulsion and rudder effectiveness is obtained.

It is found that vibratory forces measured at a cavitation number corresponding to full power are three times the corresponding values measured without

DD FORM 1 JAN 73 1473 EDITION OF 1 NOV 65 IS OBSOLETE
S/N 0102-014-6601 UNCLASSIFIED
SECURITY CLASSIFICATION OF THIS PAGE *(When Data Entered)*

cavitation. A significant reduction in vibratory force at zero rudder angle appears to be possible by moving the rudder from the present design location. The present transverse propeller-rudder clearance appears to be optimum.

ABSTRACT

Propeller induced vibratory forces acting on the rudder of a water tunnel simulation of the SEA CONTROL SHIP are measured as a function of longitudinal and transverse clearance in order to determine an optimum location. The influence of propeller-rudder clearance on steady state propulsion and rudder effectiveness is obtained.

It is found that vibratory forces measured at a cavitation number corresponding to full power are three times the corresponding values measured without cavitation. A significant reduction in vibratory force at zero rudder angle appears to be possible by moving the rudder from the present design location. The present transverse propeller-rudder clearance appears to be optimum.

TABLE OF CONTENTS

		Page
	ABSTRACT	i
	LIST OF FIGURES	iii
	LIST OF TABLES	v
	NOMENCLATURE	vi
1.	INTRODUCTION	1
2.	SHIP SIMULATION IN THE WATER TUNNEL	5
3.	EXPERIMENTAL PROCEDURE	10
4.	EXPERIMENTAL RESULTS	22
5.	CONCLUSIONS	32
6.	REFERENCES	44
	APPENDIX I Testing Facilities and Resulting Design Considerations	46
	APPENDIX II The Six Component Dynamometer	51
	APPENDIX III Water Tunnel Wake Survey	63
	APPENDIX IV Dynamic Calibration	71
	APPENDIX V Model to Ship Dynamic Similarity Considerations	76
	APPENDIX VI Computer Program for Data Reduction	84

LIST OF FIGURES

Fig. No.		Page
1	Assembly drawing of equipment mounted in the water tunnel test section	8
2	Convention used to measure phase on the Eductor output signal	16
3	Rudder lift coefficient versus angle of attack for DR=0.102 at four different clearance ratios. Uniform flow without cavitation, simulating for J for ship. Right handed propeller rotation	23
4	Rudder drag coefficient versus angle of attack for DR=.102 at four different clearance ratios. Uniform flow without cavitation, simulating J for ship	24
5	Propeller characteristics versus clearance ratio. Correct simulations for J for ship but no wake screen and σ is too high	25
6	Rudder vibratory loading versus clearance ratio, DR=0	34
7	Rudder vibratory loading versus clearance ratio, DR=0.102	35
8	Rudder vibratory loading versus clearance ratio, DR=0.204	36
9	Rudder vibratory loading versus clearance ratio, DR=0.306	37
10	Rudder vibratory loading versus clearance ratio, DR=0.102, at atmospheric pressure	38
11	Phase angle measurements versus clearance ratio at two static pressures	39
12	Rudder vibratory loading versus clearance ratio, DR=0.102, high air-content in the tunnel water	40
13	Photograph of propeller in test section during test	41
14	Photograph of the oscilloscope display of the Eductor output signal at four different clearance ratios	42
15	Typical dynamometer strain guage circuit	53

LIST OF FIGURES
(cont.)

Fig. No.		Page
16	Dynamometer before and after waterproofing of strain guage circuitry	55
17	Rudder dynamometer coordinate systems	56
18	Typical effects on the Eductor output signal due to changing "sweep duration"	59
19	Photograph of test section arrangement during wake survey measurements	65
20	(a) Handwoven wake screen	67
	(b) Complete model scale simulation of ship configuration	67
21	Photographs of (a) dynamic calibration rig	72
	(b) static calibration rig	72
22	Propeller RPM versus tunnel water speed to simulate ship advance coefficient	80
23	Static pressure versus tunnel water speed to simulate ship cavitation number	81

LIST OF TABLES

Table No.		Page
I	Average longitudinal velocity, V_x/V, ratios at 4 radii as obtained in the towing tank and water tunnel wake surveys	66
II	Rudder steady state data reduction program	85
III	Sample output of rudder steady state data reduction program	89
IV	Rudder dynamic data reduction program	93
V	Sample output of dynamic data reduction program	95

NOMENCLATURE

D	propeller diameter
R	propeller radius
V	speed
J	advance coefficient = $\frac{V \times 60}{ND}$
ρ	water density
ν	kinematic viscosity
T	propeller thrust
Q	propeller torque
K_T	propeller thrust coefficient = $\frac{T}{\rho N^2 D^4}$
K_Q	propeller torque coefficient = $\frac{Q}{\rho N^2 D^5}$
η	open water propeller efficiency = $\frac{J}{2\pi} \times \frac{K_T}{K_Q}$
F_n	Froude number
R_n	Reynolds number = $\frac{VD}{\nu}$
P_{ST}	static pressure
P_{VAP}	vapour pressure
σ	cavitation number = $\frac{P_{ST} - P_{VAP}}{1/2\rho V^2}$
F_x	force on the rudder in the x-direction
F_y	force on the rudder in the y-direction
F_z	force on the rudder in the z-direction
B_x	moment on the rudder about the x-axis

B_y moment on the rudder about the y-axis

B_z moment on the rudder about the z-axis

A rudder projected area

C_L rudder lift coefficient= $\frac{\text{Lift}}{1/2\rho V^2 A}$

C_D rudder drag coefficient = $\frac{\text{Drag}}{1/2\rho V^2 A}$

CR clearance ratio = $\frac{\text{longitudinal propeller-rudder clearance}}{D}$

DR displacement ratio = $\frac{\text{lateral rudder displacement (off CL)}}{D}$

V_T mean velocity in tunnel test section for thrust-identity propeller loading

n propeller rotational speed - revs/sec

1. INTRODUCTION

There are two main types of vibratory forces induced by a propeller. The first type is known as *bearing forces*, and consists of induced vibratory forces on the propeller caused by the incoming non-uniform wake of the ship. These forces are delivered to the hull shrough the stern bearing. The second type, known as *surface forces*, consists of induced vibratory loads through water on a structure near the propeller such as the hull or the rudder; They are caused by time dependent variations of the flow field, due to the rotation of the propeller. As a result, these latter forces may arise even if the propeller operates in a steady flow.

One should note at this point that the term *forces* is used in this context in a broader sense and should be interpreted as meaning any type of hydrodynamic excitation arising from the propeller whether this is a force or a moment.

It is clear from the above definitions that in the context of this report only surface forces are of interest. The above subdivision of propeller forces is by no means universal. Different authors use different terms. F.M.Lewis [2,3], for example , distinguishes between surface (acting on the hull surface excluding the rudder) and rudder forces.

A further distinction is often made among surface forces by subdividing them into *pitch unbalance forces* and *blade frequency forces*.

Had we had a perfectly shaped propeller operating at constant r.p.m. in a uniform axial wake then symmetry would require the generation of constant torque, constant thrust, zero lateral force variation, and zero

moment variation about any axis normal to its shaft axis.

Pitch unbalance forces and moments are generated by non-uniformities embodied in the propeller blades during manufacturing or due to blade damage occurred as a result of the propeller running into an obstruction.

The effect of such irregularities is the introduction of first order (frequency same as that of the propeller shaft) forces and moments at the propeller shaft bearing. If the propeller operates in a non-uniform wake as is usually the case with surface ships, pitch unbalance would also result in the introduction of superimposed variation effect with a first order fundamental frequency but which may have harmonic components depending on which frequencies are excited by the non-uniform flow.

Blade frequency forces exist regardless of the degree of perfection in the manufacture of the propeller. As one would expect they vary at blade frequency (equal to propeller r.p.m. × no. of blades) or at one of its harmonics.

The hull surfaces on which surface forces act are classified as *tip-clearance surfaces* and *axial clearance surfaces*. In single screw ships tip clearance surfaces are the hull surfaces above the propeller whilst axial clearance surfaces include struts, bossings, and the rudder.

The operation of the propeller in a non-uniform wake tends to increase the surface forces above the level they would have, had the inflow been uniform. These wake-induced force movements are known as wake-reflection forces.

The rudder in a single screw ship extends inside the vortex sheet flow behind the propeller, the various components of which produce vibratory forces of frequency equal to propeller blade frequency.

The study of propeller-induced rudder vibration has much more recently been developed. Its importance has been augmented as ship speeds and propeller thrust loadings have increased. Most of the relevant research has been conducted over the last decade and has frequently been related to the field of hydroelasticity.

Vibration of the rudder above a certain level may either cause local failure or may in turn excite vibration of the entire hull ("spring mass effect"). Prediction of dynamic response characteristics of the rudder to hydrodynamic loads can be of great assistance to the designer.

Although the present experiments carried out at M.I.T.'s water tunnel were trying to simulate conditions behind a particular ship, the results may be valid for other vessels too.

The ship in question, the Sea Control Ship, is a single screw, high speed, transom stern type ship. It also comprises the additional feature (which is getting quite common nowadays) of having the design location of the rudder moved slightly to the starboard of the center line of the propeller shaft axis.

The reason behind this is twofold. It causes the rudder to miss the hub vortex of the propeller and enables the propeller shaft to be removed without needing to unship the rudder every time this is desired.

In such a case maintenance or repair time can be reduced considerably which is an important advantage to ships with high availability requirements. As a result, one of the objects of the experiment was to examine whether this

special feature has a detrimental effect on the level of induced vibration or not.

One may note, however, that this feature which is getting quite usual practice on single screw ships is even more common to twin screw ships where the two rudders are not aligned with the propeller axes. Thus, the results of this experiment can be of some use to twin screw ships by giving some indication of the effect on vibrations of various transverse positions.

Since longitudinal propeller-rudder clearance is a critical parameter in determining vibratory force levels on the rudder, it is important to establish a precise definition at the outset. In accordance with current NAVSEC practice, this clearance is defined as the distance between the center of the blade when it is at its uppermost position and the leading edge of the rudder measured on a line parallel to the propeller shaft at a distance equal to 70% of the propeller radius. This definition differs from that used by F. M. Lewis [2], [3], where the distance is measured at the shaft centerline, rather than at the 70% radius.

2. SHIP SIMULATION IN THE WATER TUNNEL

Since in our experiment we were trying to investigate what happens behind a given ship, it was necessary for us to make maximum use of the information we had been given on the ship's design features and its operational characteristics.

To facilitate our task, the project sponsor provided us with drawings of the stern part of the ship, specifying the limits of the permissible changes of rudder longitudinal and transverse positions. The ship operating conditions were also given to us in non-dimensional form (by providing values of J, σ, and K_T) together with the results of the ship's wake survey.

In addition to all this information, we were given the model of the propeller. This immediately determined the model/ship scale ratio, approximately .0410, and took care of the K_T requirement.

To be able to satisfy both the J and σ requirements we made use of dimensional analysis (see Appendix V) and came forward with a set of tunnel operating conditions' options. Deciding which of these options was to be selected was left to the results of the natural frequency analysis.

Combining all the above information as well as information obtained from close examination of the ship's drawings, the design requirements of the model may be summarized as follows:

1) The model must satisfy the rudder lateral movement requirements. In other words, the rig must be such as to enable the accurate location of the dynamometer-rudder subassembly at exactly the seven predetermined positions.

2) It must also be able to simulate the slight flow inclination (~4.5°) relative to the "vertical" (i.e. normal to baseline) rudder stock (here modelled by the dynamometer). At present, however, the tunnel's propeller drive system does not allow for changes in the shaft angle. As a result, the propeller shaft must be horizontal and the rudder dynamometer must bear the inclination. Either way would produce similar results.

3) The supporting rig must permit changes in the angle of attack (rudder deflection).

4) The model must allow for variations in the axial propeller-to-rudder clearance. One should note that "clearance" here is defined as the distance between the centre of a blade, where it is at its uppermost positions, and the leading edge of the rudder measured on a line parallel to the propeller shaft centerline and at a distance equal to 70% of the propeller radius, R.

5) It must also be made watertight whenever leak paths are anticipated.

6) The supporting rig must be rigid enough to allow for very small axial and lateral displacement of the assembly.

7) The model must incorporate certain appendages (in the form of screens) which will simulate the ship's axial wake as closely as possible.

8) All positions and angular changes must involve a minimum number of adjustments.

9) Finally, the model must have a natural frequency lying above the anticipated operating blade frequency.

A description of the final version of the model is given in the following section. The various considerations that led to it however, are discussed in more detail in Appendix I.

Description of the Model

A view of the model is given in fig.(1). The aluminum window is bolted down to position on the tunnel. A thick steel plate (the "infinite mass") is bonded unto the window by means of a 9/16" thick layer of ECCOBOND epoxy mixture (2 parts ECCOBOND to 3 parts of catalyst by weight). This method of attaching plate to window was chosen as our final attempt to decrease the system's natural frequency by lowering its stiffness.

The dynamometer is held into position by a massive aluminum clamp bolted on top of the steel plate. Lateral movement can be achieved by allowing the clamp to move inside a groove cut out in the plate. The clamp must be sufficiently large to cover the entire groove at all positions. Note that the groove is large enough to ensure access to 1/2 the lateral positions required. The other half can be obtained by rotating the window 180°. This method,although time consuming, has two great advantages. It wastes a minimum amount of steel mass and requires a smaller clamp.

The rudder is held tight against the tapered bottom end of the sensor. A "tiller" used for angular adjustments is fixed on top of the dynamometer. Whenever a change in angle of attack is to be made, the clamp is slightly loosened and the rudder assembly is rotated to its desired position. A tapered pin sliding through two holes on the tiller and the clamp, prevents any further movement.

Sealing is provided by an O-ring between the steel plate and the clamp and another O-ring and a gasket between the jaws of the clamp.

To further simulate the ship's hull by providing the proper propeller tip clearance, it was found necessary to use a splitter plate. This is

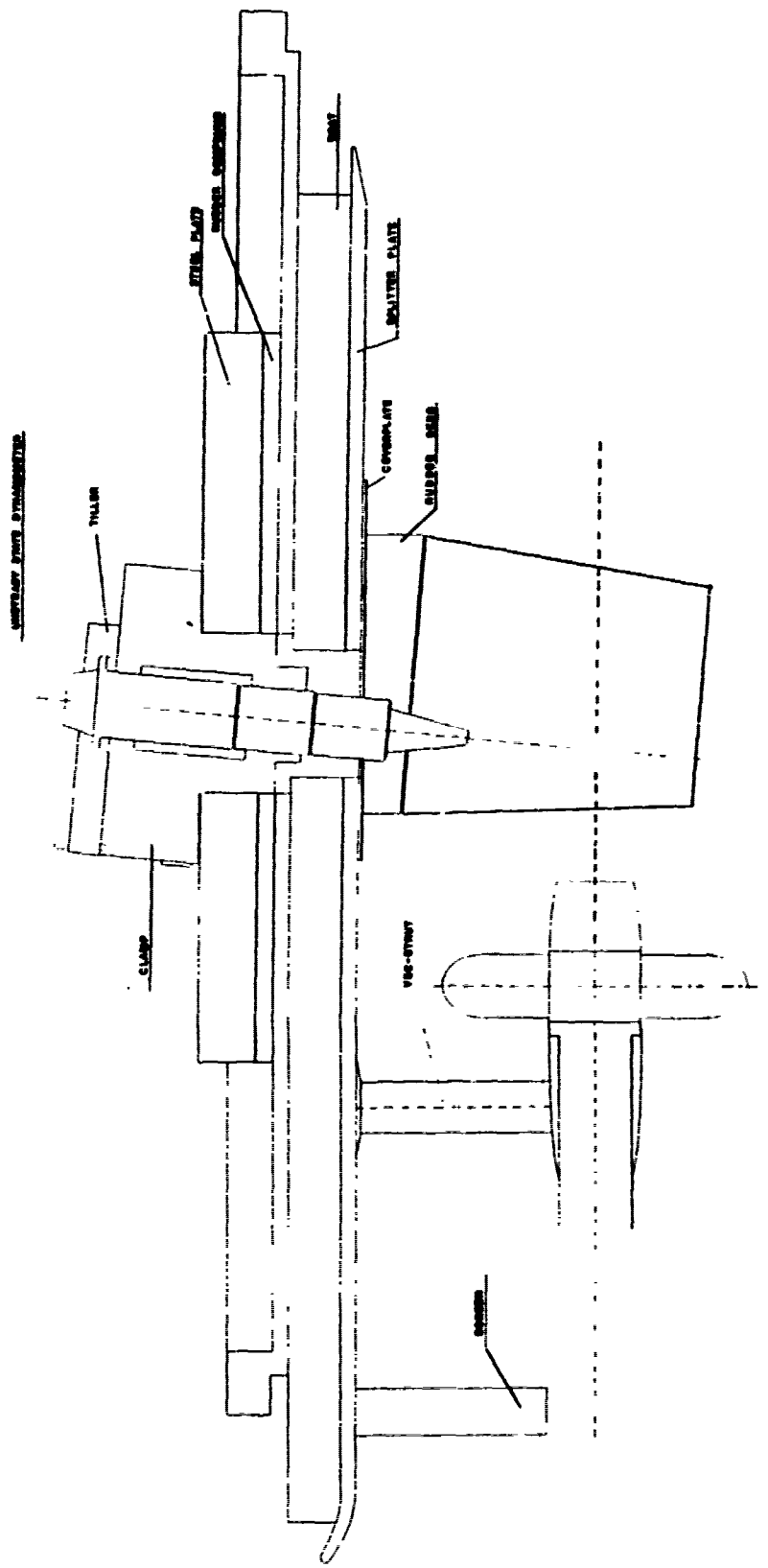

Fig.1: Assembly drawing of equipment mounted in the water tunnel test section

held into position 1 3/4 inches from the top of the test section by means of an aluminum streamlined *boat*. Like the steel plate, both splitter plate and boat have a transverse groove cut into them to allow for sideways movement of the clamp-dynamometer subassembly. The splitter plate extends across the whole width of the test section leaving practically zero-clearance at the sides to ensure the complete splitting of the flow above and under the plate.

Although the splitter plate is longer than the previous one used for other experiments in the tunnel[9], it still extends less upstream than the test section wall and thus manages to reduce the boundary layer thickness (see Appendix III). Finally, to avoid flow separation, the leading edge was faired as shown in fig.(1).

The groove in the splitter plate is covered by means of a set of interchangeable coverplates, one of which carries the rudder skeg (fixed part of the rudder). The skeg proportions had to be altered slightly to make it possible for the dynamometer to go through it with clearance.

The vee-strut assembly slipping over the propeller shaft is used to simulate the strut on the ship. Three set screws holding it tightly against the drive shaft housing make sure that it remains at a constant distance from the propeller as the longitudinal position of the latter is changed.

Finally, to simulate the non-uniform wake behind the ship, it was decided to introduce in the flow a wake screen, attached near the leading edge of the splitter plate, capable of creating a velocity profile similar to that of the ship. The variable solidity of the screen as a function of distance from the propeller shaft centreline was developed in a wake survey carried out in the tunnel described in Appendix III.

3. EXPERIMENTAL PROCEDURE

Although we were primarily interested in examining the effect of propeller to rudder orientation on the vibratory loading of the rudder (dynamic tests), it was found worthwhile to extend the investigation a step further to include the effect on the steady state characteristics of both propeller and rudder (steady-state tests).

This decision was taken in order to ensure that the longitudinal and lateral position of the rudder, with respect to the propeller, the dynamic tests would indicate as being the "optimal", would not have a detrimental effect on the steady state performance characteristics.

Thus, the overall experiment was divided into two main parts, the first dealing with dynamic tests and the second with steady state tests. For simplicity these are treated here separately.

Dynamic Tests - Modifications to the Original Plan

By the time we started the first tests, in early July 1974, we had already decided to modify our original testing plans. It was then that we decided to examine only the centreline and starboard lateral positions of the rudder, based on indications obtained after the first test runs, that the optimum lateral position was near the design value (which corresponds with 1" to the starboard on the model). This decision was also enforced by another consideration. Obtaining the port lateral positions (as already described) meant rotating the window by 180° and refastening it on the boat. Because of the absence of symmetry in the shape of the boat this last step would inevitably involve drilling a new set of

holes into the window, thus increasing the number of possible air-leak paths into the system which we knew would hinder our experiment.

After a number of trial runs, we discovered that there was little advantage gained by using a smaller increment of longitudinal movement of the propeller near the design position (at a clearance ratio of about .57). Instead, one centimeter intervals were used throughout the travel of the propeller with the only exception that in the three last points (at very large clearance ratios) the increment was increased to two cms.

The final change involved the investigation of the effect of changes in angle of attack on the vibratory loading of the rudder. For reasons explained in Appendix II, we were not able to get any results at angles of attack greater than 5°. As a result, our original plans for a thorough investigation of this effect had to be abandoned.

Dynamic Test Procedure

With the rudder, at one of the four lateral locations to be investigated, the tunnel was first run at a low water speed and a static pressure close to the desired testing value (236-mmHg) in an effort to drive as much air out of solution as possible. The air thus released was gathered in the vacuum chamber at the top of the tunnel, and upon further reductions in pressure, was driven completely out of the system.

After a period of time varying between 20 minutes and 1 hour, both the propeller r.p.m. and the tunnel water speed were increased until the desired testing values were attained (1500 r.p.m. and 17.3 ft/sec respectively). Some additional time was then allowed for the tunnel to reach equilibrium at these new conditions during which frequent adjustments were necessary.

Once equilibrium was reached, a fact which was verified by the lack of fluctuations in the level of the "blue fluid" inside the manometer, we were able to start taking readings.

For all the dynamic tests involving 0° angle of attach the dynamometer amplifiers' gain was set at its maximum value. This was done in anticipation of the fact that the expected steady state loads at 0° rudder angle, were not large enough to cause saturation of the amplifiers. Nevertheless, the two dynamometer response signals F_z and B_x were examined prior to being averaged, were viewed on an oscilloscope (TEKTRONIX model 561B) and a biasing voltage was applied whenever necessary. After this check for saturation, the two response signals were supplied, one at a time (via a six-way switch), to the waveform eductor "signal input" jack. A detailed description of the dynamometer and the waveform eductor is given in Appendix II.)

A switch on the eductor's front panel is used to select one of the three possible operating modes of the instruments. In the "analyze and readout" mode the instrument simultaneously samples the input signal, stores the repetitive synchronized component of the signal in its memory and supplies the contents thereof to the output. With a characteristic time constant, τ, set at 20 secs, it took the eductor approximately 2 minutes to analyze and store the input signal. At the end of the 2 minutes, the mode switch was turned to the "readout only" position. In this mode no further sampling of the input signal takes place, but the instrument simply scans its memory and supplies the contents thereof to the output. Such a signal was used to drive the oscilloscope which was triggered externally with the "gate signal", which is a positive pulse available for the duration of each sweep, at the gate jack on the eductor's front panel. An oscilloscope

camera (TEKTRONIX model C-59) was then used to make a permanent record of the output response. After the picture was taken, the signal was erased (by turning the mode switch to the"erase" position) and then the whole cycle was repeated for the second dynamometer signal.

In order for the eductor averaging sweeps to be synchronized with the rotation of the propeller an external trigger pulse had to be supplied to the "trigger in" jack. This was accomplished using a magnetic pick-up, located at the rear end of the propeller drive, which activated a spike generator everytime a tooth of the five-tooth gear rotating with the shaft, passed over it. With a five-tooth gear and an appropriate sweep duration (about 7.8msecs) it can be arranged so that the eductor examines the input signal five times per propeller revolution. This provides a better system response criterion since the eductor will, at each sweep, integrate the input signal with a different blade at a particular position so that individual blade non-uniformities will be removed in the averaging process. One should note that the two pulses, the one triggering the eductor and the one available at the "gate" jack are perfectly synchronized.

After one full run was completed (there were approximately 17 longitudinal positions per run) a check for repeatability was undertaken. This was in fact nothing more than a repetition of the readings previously taken, at randomly chosen points. It was during one of these checks that we discovered how amplifier saturation could affect our readings as well as the importance of high air content in the water. After we satisfied ourselves that the readings originally taken could be reproduced we would go on and change the lateral position of the rudder.

When all the four runs were completed we decided to make two additional runs. The first one was a repetition of a complete run previously carried out during which the air content of the water had been unusually high and for which the results from the check for repeatability had not been completely satsifactory. The results this time were much better and easily reproducible but had little similarity with the ones originally obtained.

The second additional run was at the same J as for the ship but at a different value of σ. The value chosen, σ=7.0, corresponded to atmospheric pressure in the tunnel. At such pressure there is no cavitation and the resulting loads as we expected were much smaller.

Finally, we started testing for changes in angle of attack (rudder deflection angle). For these tests, due to the increase in the load, the amplifier gain had to be dropped to its minimum value. Nevertheless, saturation of the amplifiers made it impossible for us to get results for rudder angles greater than 5°. We thus checked the effect on the vibratory loading of changing the angle from -5° to +5° at two different longitudinal clearances and at the design lateral position. We were unable to test at any additional point because the waterproofing, subjected for such long periods to low pressures and high water speeds deteriorated and was no longer able to prevent water from penetrating the guaged area of the dynamometer and damaging the circuitry.

The results of all the tests described are discussed in greater detail in the next section.

Reducing the Dynamic Data

After a run had been completed the data obtained was reduced using the "dynamic data reduction program". This program consists of two parts.

In the first part, the program makes use of the results obtained in the dynamic calibration (see Appendix IV) to develop a matrix of the complex influence coefficients. This matrix is then used in the second part of the program in the reduction of the data obtained during the experiment. The final output is given in non-dimensional form as force and moment coefficients. In both parts of the program the input consists of the amplitude and phase values of the recorded signals of the two channels obtained at a given point.

The amplitude of the signal is equal to half the peak to peak value directly measured on the photograph multiplied by the sensitivity of the scale.

The phase, on the other hand, is taken as the fraction of the cycle in degrees by which the positive peak of the signal leads "zero phase". This "zero phase" is arbitrarily taken as occuring exactly at half the interval between two consecutive triggering spikes. At this instant (it was arranged by carefully setting the five-tooth gear position, relative to the propeller) a propeller blade is always located at its uppermost position. The way phase is measured is better illustrated in fig.(2).

All the dynamic test reduced data is given in graphical form in the next section whilst a listing and a sample output of the "dynamic data reduction program" is given in Appendix VI.

Steady State Tests

As already stated, the steady state tests were carried out more as a complement to the dynamic tests than to investigate in detail the steady

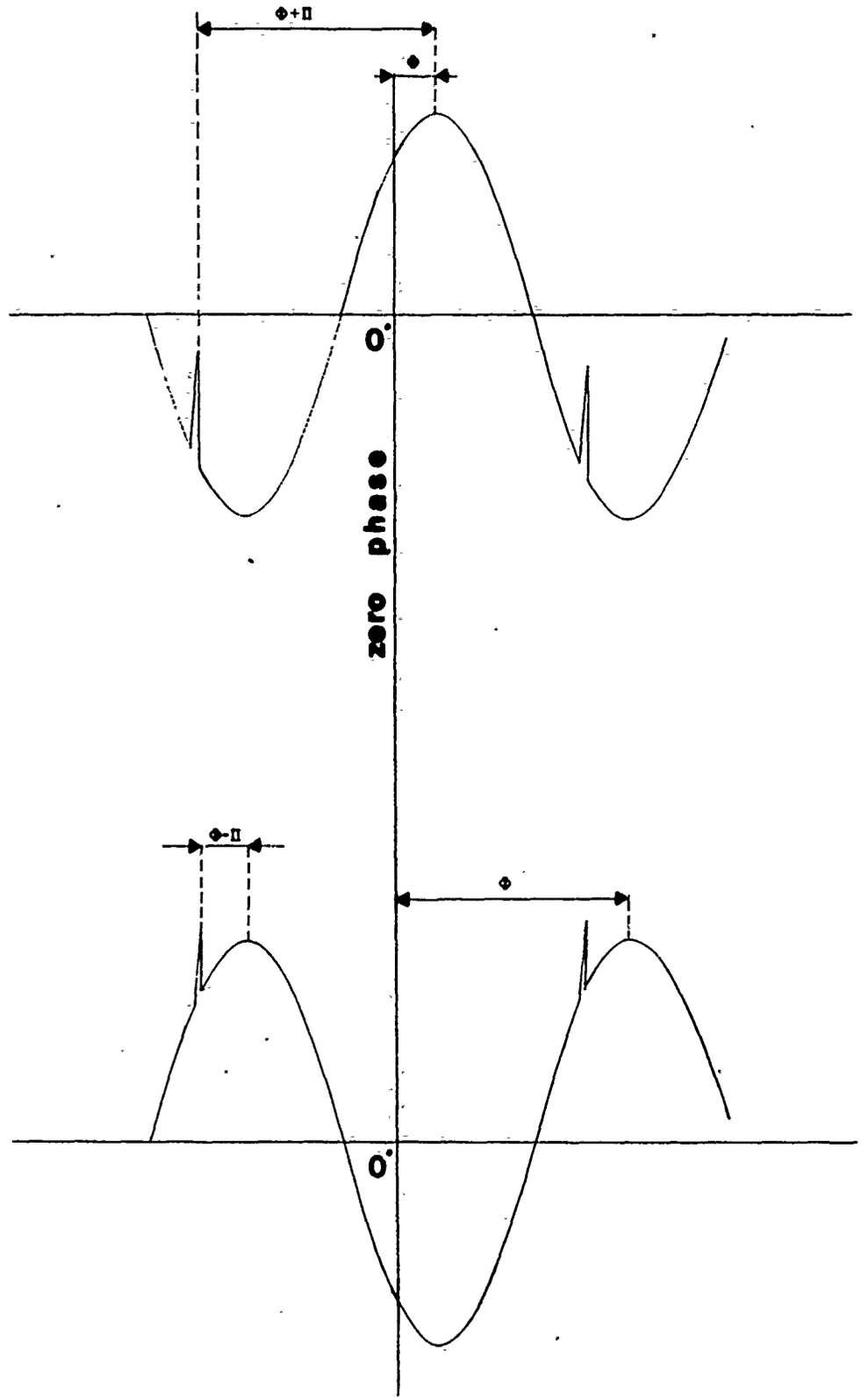

Fig.2: Convention used to measure phase on the Eductor output signal

state characteristics of both propeller and rudder.

The main reason behind such an attitude towards steady state tests was that with the dynamometer at its present form, there was not much more that we could do. A further reduction in gain, which would have undoubtedly increased our testing possibilities, involved tampering with the electronics of the dynamometer which was not feasible under the present project.

Thus, as soon as we discovered that the steady loading on both rudder and propeller was unaffected by changes in clearance the steady state tests were discontinued and we concentrated on effects on dynamic testing.

The testing conditions during these tests were also quite different from the ones just described. First, the cavitation number being so low, even at the smallest amplifier gain, it was impossible to obtain results at rudder angles greater than 10°. Furthermore the amount of cavitation appearing on the leading edge of the rudder indicated that changes in the tunnel pressure would have no measurable effect on the steady state loading. Thus, our first decision was to increase the pressure in the tunnel to "atmospheric" where we knew that no cavitation would occur and as a result the dynamic loads on the rudder would be greatly reduced.

Even at a pressure as high as this, however, we were still unable to take any readings when the angle of attack exceeded 20°, without saturating the amplifiers. As a result, at such angles, in order to decrease the rudder loading, we decided to reduce the values of both n and V_T, keeping their ratios constant (for constant J) but effectively changing once again the value of σ.

The second testing condition that was altered was the fact that no wake screen was used. There are two main reasons behind this decision. The first one is that at the time we carried out these tests there was no

one is that at the time we carried out these tests there was no

wake screen available; the prototype had failed and we were in the process of constructing the second (handwoven) version (see Appendix III). The second reason was that we felt that the presence of a screen would not significantly alter the influence of propeller to rudder clearance on the steady loading

Rudder Tests

Had it not been for the significant reduction in the amplifier gain, the input signals used in the steady load analysis would have been in no way different from the ones used for the dynamic tests. In fact, if we had performed a static calibration of the strain gauges, with the various amplifiers set at their maximum gain, nothing (except probably lack of time) would have prevented us from carrying out dynamic and steady state tests simultaneously.

The differences in the two tests lie in the way these signals are analyzed as well as on the fact that for steady state tests we examined the output of five rather than two dynamometer channels.

The instrument used to measure steady loads on the rudder was a digital indicator (LEBOW ASSOCIATES model 7521). This instrument was originally purchased to be used in conjunction with the load cells which are part of another steady state dynamometer used in propeller tunnel as well as open water tests at M.I.T. To analyze these steady state loads this instrument incorporates a transducer unit which provides the excitation voltage to the load cells and later amplifies and filters their output signals

prior to digitizing them. The filter and the digital voltmeter were the only parts necessary in our case and we had the instrument modified by the addition of another unit (essentially a two-way switch) to allow us to by-pass the transducer circuit. Thus, the indicator could be used as a digital voltmeter with the additional feature of being able to filter the input signal prior to digitizing it. Thus, by allowing a very narrow band of frequencies to pass through the filter, the fluctuation of the readings would be kept to a minimum and we had no problem isolating the steady components of the dynamometer output signals. A high degree of filtering, however, required a lot of damping which in turn meant that a considerable amount of time had to be allowed before being able to take any readings.

There was one additional consideration we had to take into account before using this instrument for the analysis of the signals. This is the ± 1 volt limitation on the input signal voltage imposed by the instrument's circuitry. On the other hand, we knew that the output from the amplifiers could be as much as 15 volts (the saturation voltage which is independent of gain). Thus allowing for a safety margin we introduced a voltage divider into the circuit in the six-way switch capable of reducing the amplifier's output voltage to 1/17 of the original value. The reduced signal was then presented to the digital indicator at the "J_1" inlet located at the rear panel of the instrument.

Rudder steady state tests involved measuring the output of five out of the six dynamometer channels for thirteen values of rudder angle (from +30° to -30° at 5° intervals) and at four longitudinal clearances between

propeller and rudder. Only one lateral position was examined (the design position). The output of the sixth dynamometer channel was of no interest to us because it measured vertical forces on the rudder which for all practical purposes are negligible. Prior to doing any testing a static calibration was performed to evaluate a matrix of influence coefficients relating the applied to the read values of the various loads (see Appendix IV).

To be able to obtain readings at large angles of attack the no-load input voltage to the amplifiers had to be biased. Because of the reversal in algebraic sign of three out of the five loads, we were measuring, (F_z,B_x, and B_y), as we moved from positive to negative rudder angles it was clear that the same no-load bias could not be used throughout the test without saturating the amplifiers. As a result the rudder steady state tests had to be divided into two groups, one dealing with positive angles and the other with negative. In order to move from one group of tests to the other both n and V_T had to be turned all the way down to zero and the no-load values of the voltage inputs to the amplifiers of the three channels were reversed.

The amount of bias corresponding to each amplifier was read on the digital indicator and constituted the "zero reading" value of each channel as used in the "steady state data reduction program" (see Appendix VI).

Propeller Steady-State Tests

These tests were carried out simultaneously with the rudder tests and for the same tunnel conditions and number of points. The propeller thrust and torque were measured by two different load cells coming as one package designed and built to be used in this propeller tunnel. Due to the pro-

peller rotation the load cells output signal is transmitted to the digital strain gauge indicators (LEBOW ASSOCIATES model 66) through slip rings. These indicators are calibrated so that they measure thrust and torque directly so that no further calibration was needed. A computer program program (not included here) is then used to reduce the data obtained giving as output a set of non dimensional coefficients including K_T, K_Q, and efficiency η.

4. EXPERIMENTAL RESULTS

Steady State Tests

The results obtained in the steady rudder experiments were very much like we had expected. There was no change to speak of, in the steady state loading at any of the four longitudinal clearances we investigated. The lift and drag coefficients C_L and C_D are plotted against rudder angle at four clearance ratios. The four curves almost completely coincide (see figs.(3,4)). As already stated in the preceding chapter onl· the design lateral location of rudder was investigated (design lateral corresponds to a displacement ratio, DR, equal to .102).

One should note that both plots indicate quite distinctly that zero lift, and hence minimum drag, do not occur at exactly 0° rudder angle but at some other negative angle. This is not unusual but actually quite common to all ships with an odd number of propellers or any number of unirotating propellers. These ships in order to be able to sail a straight course must set their rudder at some angle other than 0°.

Similar conclusions can be derived from the propeller steady state tests. Propeller thrust coefficient, K_T, torque coefficient, K_Q, and efficiency, η , are all plotted versus clearance ratio. None of these quantities appears to have changed to any observable degree with propeller to rudder clearance, (fig.(5))

We can thus conclude at this point that whatever the decision on the final position of the rudder, it will have to be made on the basis of the results of the dynamic tests alone since no constraints appear to be imposed by steady state loads.

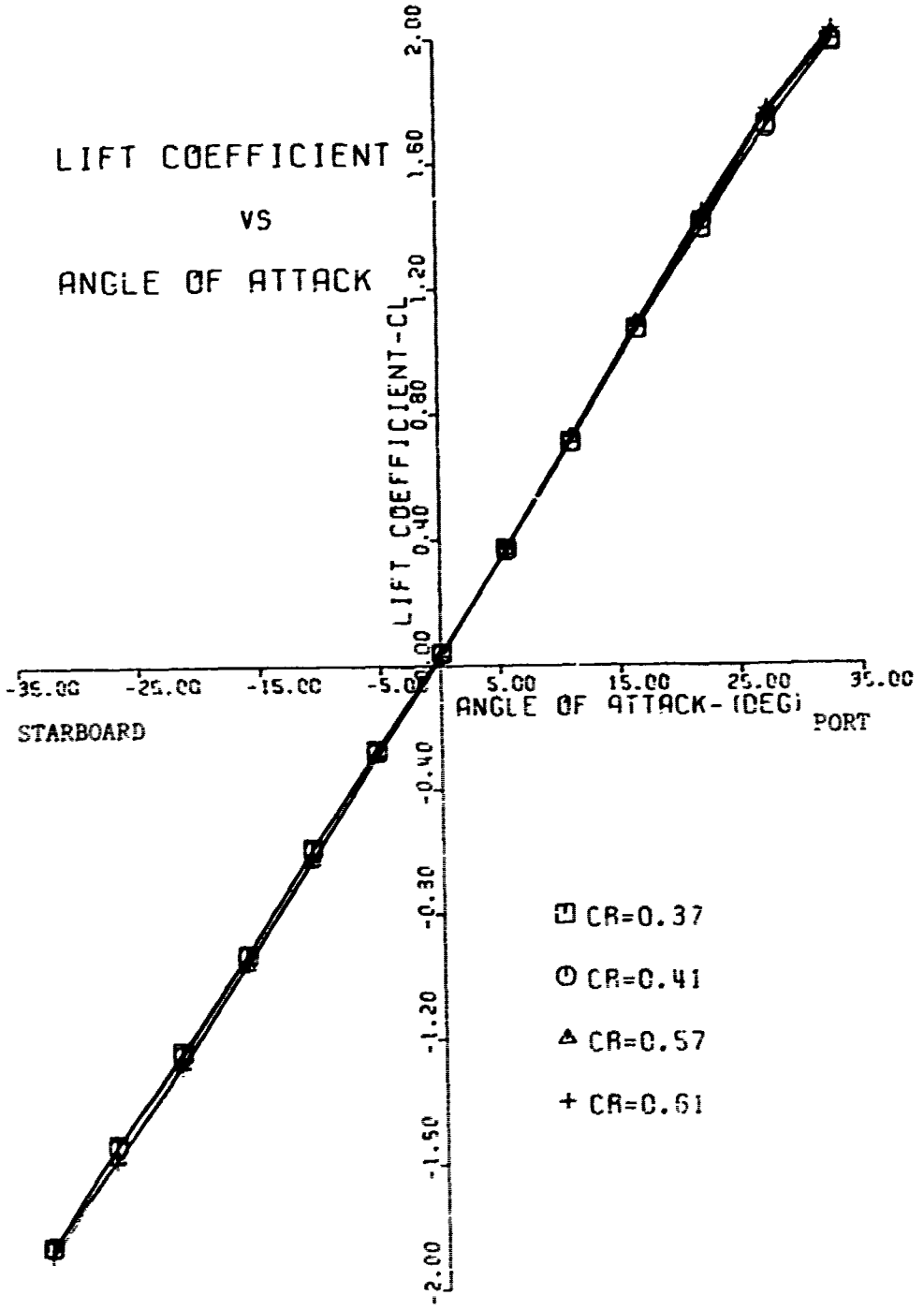

Fig.3: Rudder lift coefficient versus angle of attack for DR = 0.102 at four different clearance ratios. Uniform flow without cavitation, simulating J for ship. Right handed propeller rotation.

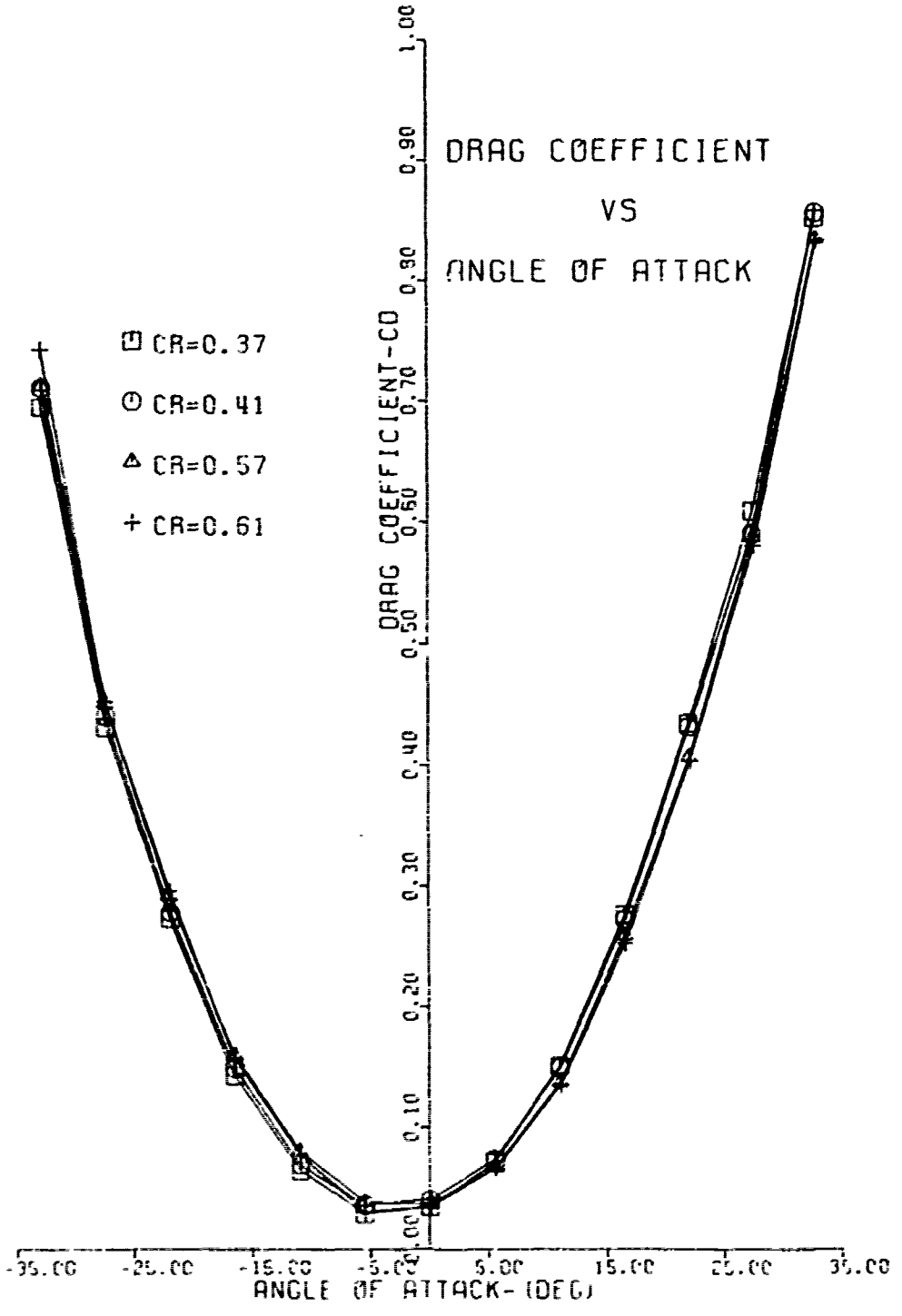

Fig.4: Rudder drag coefficient versus angle of attack for DR=.102 at four different clearance ratios. Uniform flow without cavitation, simulating J for ship.

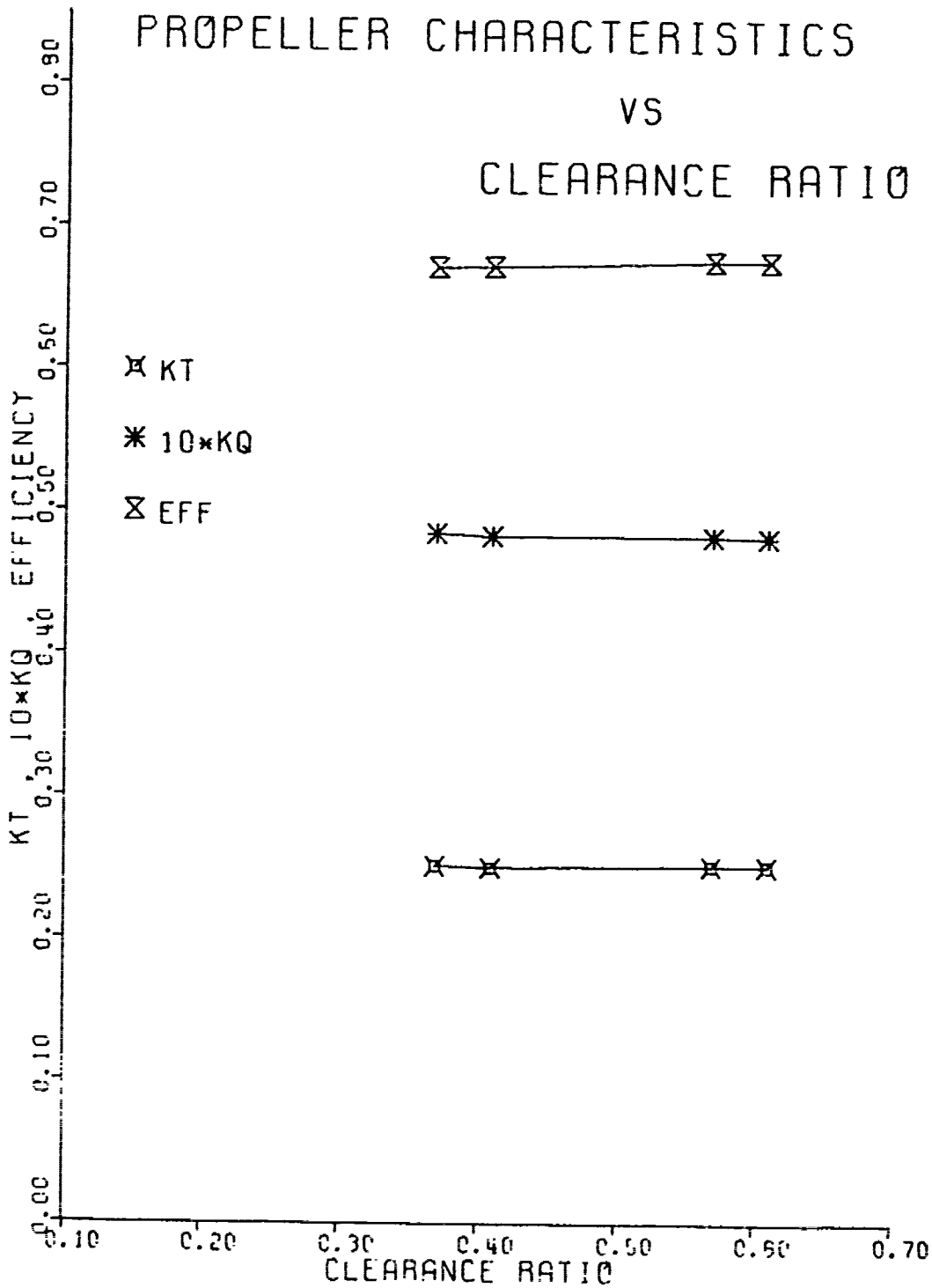

Fig.5: Propeller characteristics versus clearance ratio. Correct simulations for J for ship but no wake screen and σ is too high.

Dynamic Test

The results obtained in the dynamic tests are given graphically on figs.(6-12). The first four plots, one at each lateral location, are for the same tunnel operating conditions and in all of them the model to ship dynamic similarity requirements are satisfied.

The air content of the water is kept to as low a value as possible by going through the procedure described previously under Dynamic Test Procedure. It was, however, impossible for this deaeration procedure to have exactly the same results each time, so that reservations to compare the results of these runs at face value may be justifiable. Nevertheless we did try to keep the air-content to a minimum each time so that comparison is possible. As a result we see that there is an overall drop in magnitude of the loads as we displace the rudder laterally from directly behind the propeller (DR=0). These loads reach a minimum somewhere between 1" and 2" off the model centre-line (.102<DR<.203) and then start again increasing as we move farther to the side.

This change in the loading may be interpreted as follows. Exactly behind the propeller, the rudder is swept by the propeller hub vortex and the induced velocities create a fluctuating pressure field which increases the vibratory loading on the rudder. The farther away we are from this hub vortex the smaller its effect on the resulting loads until we reach a point where the proximity of the tip vortex envelope causes a similar effect.

When we consider each run separately we see that the probability of the air-content of the water changing within its duration is very small.

Nevertheless, we decided to reduce this probability even more by the addition of about two inches of water to the top of the tunnel, thus covering entirely the top window. This was done because earlier tests had indicated that this window was the major source of air-leak paths into the tunnel.

It is quite clear from the graphs that there is a substantial variation of both the force and the moment coefficients (K_F and K_B respectively) with changes in the longitudinal clearance ratio, CR. One may note at this point that these curves agree quite well with those of previous experimental work. [5,6]

Close inspection of the curves indicates that the peaks of the forces and moments occur at more or less constant intervals, a fact suggesting that there is a definite relationship between these values and the pitch of the tip vortex helix. The fact that all four curves agree in that respect strengthens this view. The pitch/no. of blades of the helix as measured on a photograph (fig. 13) is approximately 5.1 cms, which corresponds to the size of the interval between consecutive peaks on the curves.

In other words, maximum vibratory loading on the rudder appears to occur whenever the tip vortex helix "cuts" the rudder at a particular point. Where exactly this point is located it is hard to tell. Had we taken a series of photographs of the tip vortex impinging on the rudder at all the clearance ratios it might have probably been possible to determine the exact correlation between the point of incidence and the peaks of the curves. Unfortunately, this was not done.

There is, however, an additional consideration apparently not satisfied

by this interpretation, which suggests that there might be an additional source of excitation of these loads. This is the fact that the phase of the response signal appears to be nearly independent of the distance between propeller and rudder (see fig. 14).

Another very likely source of vibration is the passage of a blade behind the wake screen five times per propeller revolution (i.e. at blade frequency). This means that five times per revolution the loading on the propeller changes due to the different velocity field existing behind the wake screen. As a result of this, a pressure wave is generated on each blade which travels at acoustic speed and induces vibratory forces on the rudder. Because of such high speed, the few centimeters between the various points are immaterial to the time it takes the wave to reach the rudder. Had this been the only source of excitation of vibratory loads on the rudder then one would not expect any change in the phase of the response signal.

But we have already interpreted the peaks of the curves as occuring due to the tip vortex striking the rudder at different points. So it seems quite likely that the total loading on the rudder should result from a combination of the effects of the two sources. The net load on the rudder would then be a vector sum of the two different loads. The loads generated by the presence of the wake screen, being predominant, fixes the value of the phase and the mean level of vibration, whilst the load generated by the tip vortex is the cause for the fluctuations thereof, namely the peaks and troughs of the response signals.

Things change considerably when the tunnel pressure is increased to "atmospheric". One should note that "atmospheric pressure" in the tunnel

occurs when the tunnel static pressure equals the barometric pressure plus the hydrostatic pressure of 5 feet of water (the distance from the top of the tunnel to the centreline of the test section). The results obtained at this pressure are shown in fig.(10). From this graph we can immediately observe that the overall shape of the curve has changed considerably, there is now only one peak much less pronounced than before, and that the mean level of vibration has dropped to about 1/3 of its value at low pressure (c.f. fig. 6).

The photographs of the response signal also show another difference. Now the phase changes with clearance [see fig. (11)]. It actually appears that the phase goes through a complete cycle for a change in longitudinal clearance of approximately 5cms (equal to pitch/no. of blades of the helix of the tip-vortex).

One can thus conclude that at increased cavitation numbers the vibratory loads generated by the blades crossing the variable wake field are no longer predominant and as a result of that the contribution of the tip-vortex induced forces has increased.

One should note at this point, that even though it is not visible at high pressure, the tip vortex is always present, except when the propeller is delivering no thrust. With increasing propeller loading the vortex increases in intensity and its core starts becoming visible when the pressure at the centre is reduced until it reaches vapour pressure.

An extreme case of the effect of high air-content in the water can be observed from direct comparison of fig. (7) and (12). Both runs were carried out under the same tunnel operating conditions but in the

later case the air-content was so high that the propeller was barely visible in the tunnel. Even though the peaks and troughs occur at approximately the same values of clearance ratio the plots show considerable differences in the overall shape of the response curves.

Further insight can be obtained from the photographs of the response signals. There we noticed that the repetitive part of the signal, when the air-content was high, was almost completely devoid of higher order harmonics of blade frequency and the resulting repetitive waveform was almost a pure sinusoid. This, however, was not the case when the air-content was low, suggesting that air tends to dampen higher harmonics and that the results of fig.(12) are essentially the pure blade frequency components of the signal, at the different clearance ratios. We do not know, however, to what extent this is true, and the idea of pursuing this study to find out what happens at intermediate values of air-content was almost immediately abandoned on the grounds that we had no means to either control or measure the quantity of air in the tunnel. As a result we concentrated our efforts to operate at as low an air-content as possible thus obtaining the response of the dynamometer to all the components of the propeller excitation.

Higher order harmonics of blade frequency, however, introduce an additional problem. Due to their presence the response signal was frequently distorted to an extent where phase was not always easy to determine. This was particulary the case at clearance ratios corresponding to the two smallest clearance ratios (CR equal to .33 and .37) and the two largest (CR equal to 1.01 and 1.09). In all these cases the signal was considerably distorted

to the point that the location of the positive peak (to which phase was measured) was not well defined. More than once the response signal had two positive peaks. This probably explains the differences in the shape of the four curves at these extreme points.

The results from the dynamic tests investigating the effect of changes in rudder angle are not very instructive. Due to amplifier saturation, which was caused by a considerable increase in the dynamic loading of the rudder, we had the opportunity of examining only three rudder angles ($\pm 5^\circ$ and 0°) at two clearance ratios (.57 and .77). At both positions a minimum occurred at 0°.

5. CONCLUSIONS

1. The results of these experiments indicate clearly that propeller induced vibratory forces are strongly influenced by propeller cavitation. The growth and collapse of cavitation on each blade as its passes through the high wake region generates a pressure field which increases the rudder vibratory force by a factor of three, and completely alters its phase. Realistic design estimates of vibratory force levels must therefore be based on experiments or theory in which the unsteady cavitation characteristics of the propeller are properly accounted for.

2. The vibratory force on the rudder is critically dependent on the longitudinal clearance between the propeller and rudder. For the particular design studied, the design clearance ratio of 0.57 coincided with a local maximum. A reduction in vibratory force by a factor of ten could be achieved either by reducing the clearance ratio to 0.41 or increasing it to 0.68.

3. Transverse clearance between the propeller and rudder also influences the vibratory force level. In this case the design value of DR = 0.102 appears to be a good choice. Vibratory forces are increased both for smaller and larger values of the transverse clearance.

4. The vibratory force on the rudder at zero angle of attack at full power has an amplitude of approximately 14,000 lbs. at the design location. In the absence of a structural resonance, this force is not likely to cause problems since its magnitude is only about 2% of the maximum steady designed

force on the rudder. However, any structural resonances of the rudder itself, of the steering system or of the adjacent hull structure at blade frequency or twice blade frequency could result in vibration problems.

5. Steady state propeller and rudder characteristics are relatively insensitive to longitudinal clearance within the range of practical possibility. Consequently, a reduction in clearance ratio to 0.41 to reduce the vibratory force can be accomplished without reduction in propulsive efficiency or steering effectiveness.

6. There is reason to believe that the vibratory force on the rudder may increase by an order of magnitude at large rudder angles. We were just at the point of acquiring data under these conditions when the strain gage waterproofing failed. Repairing the waterproofing and setting the experiment up in the tunnel was unfortunately not feasible within the existing project.

7. The shaft inclination of the actual ship was not modelled in this experiment since the existing propeller drive can only be located along the tunnel centerline. It was anticipated that this would introduce some uncertainty in interpreting longitudinal clearance. However, there is a further problem associated with effect of shaft inclination on unsteady propeller cavitation. Since we now find that unsteady propeller cavitation is a major variable, the present data, run with zero shaft inclination, may underestimate vibratory forces.

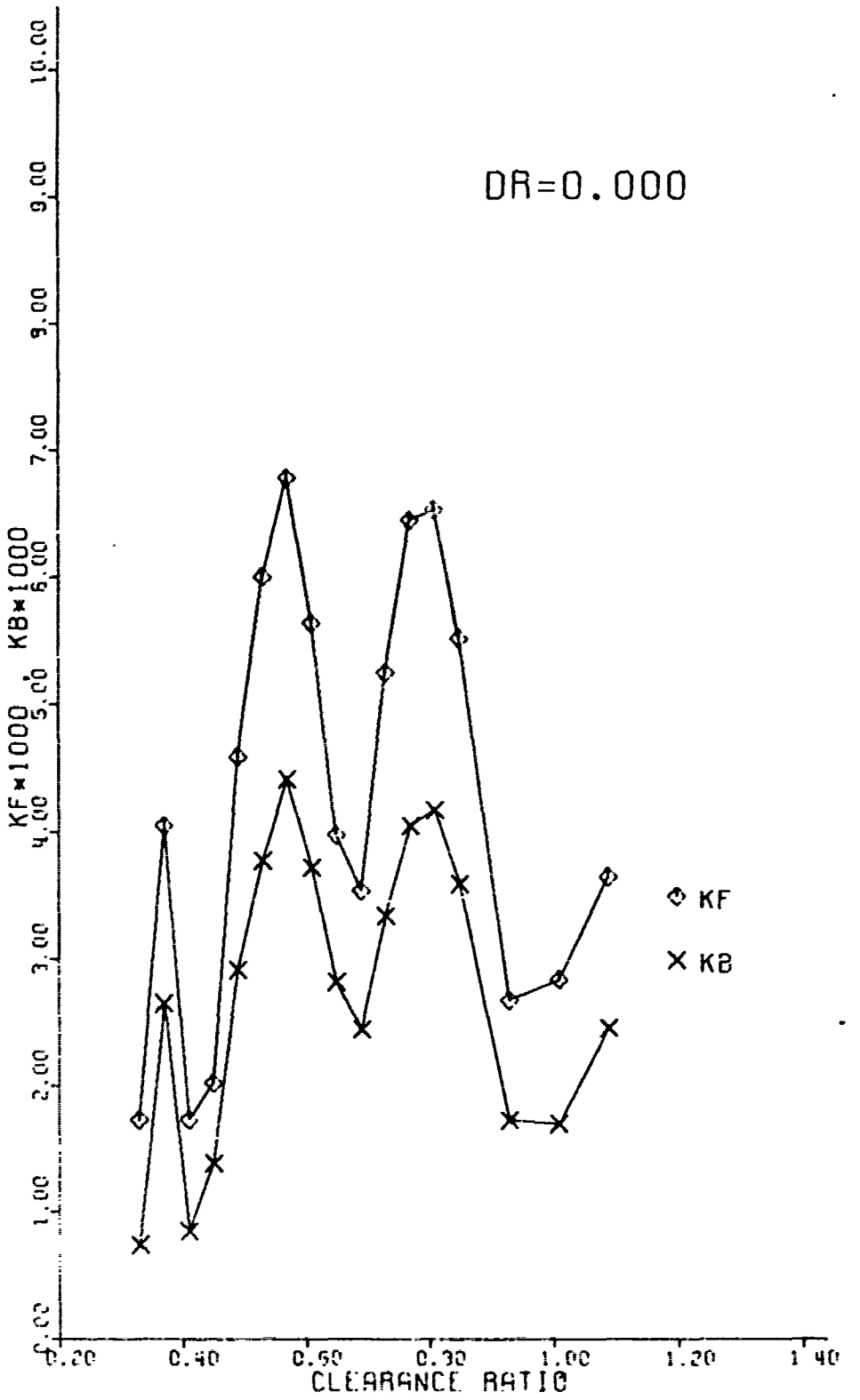

Fig. 6 : Rudder vibratory loading versus clearance ratio,DR = 0

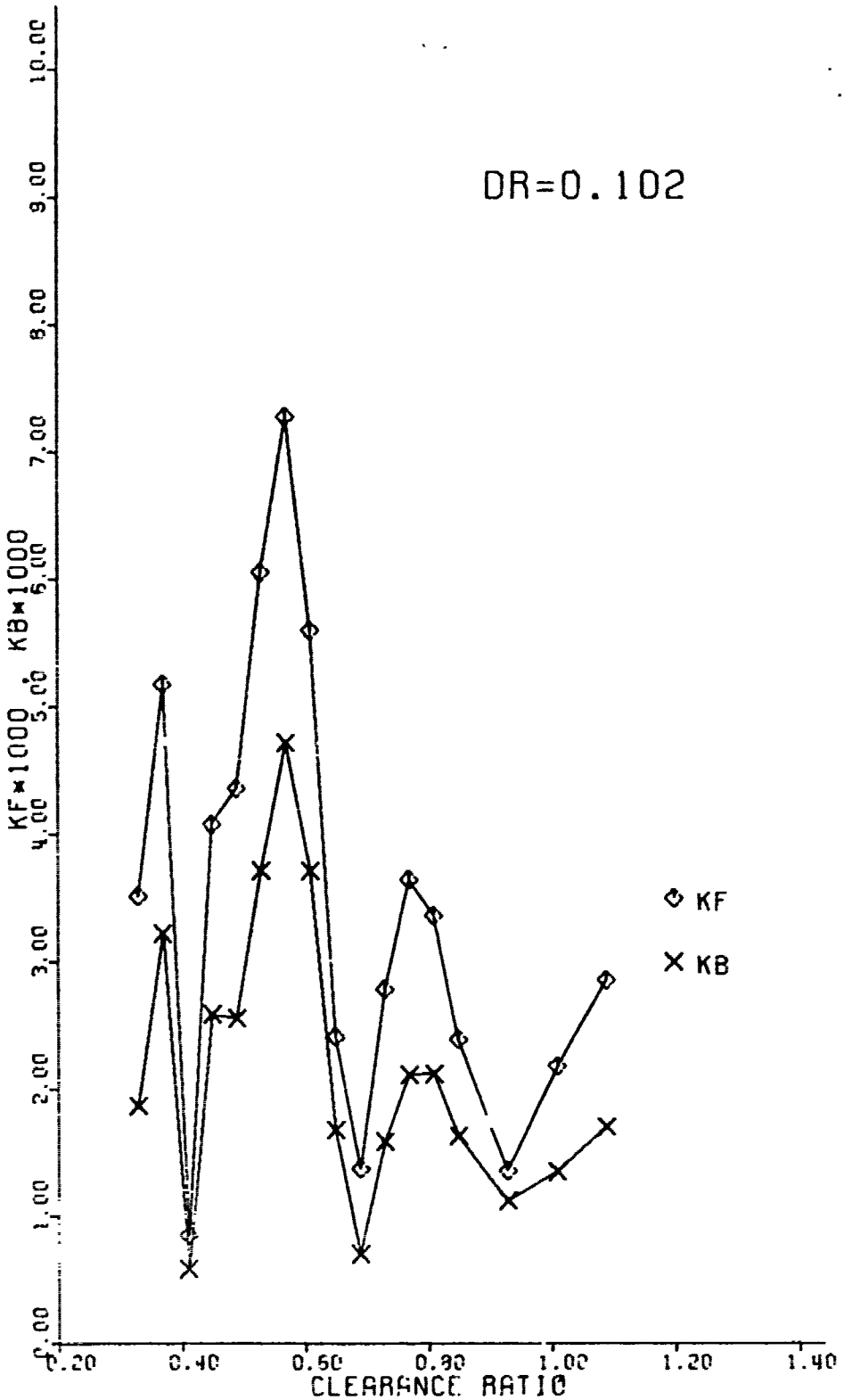

Fig. 7 : Rudder vibratory loading versus clearance ratio,DR=0.102.

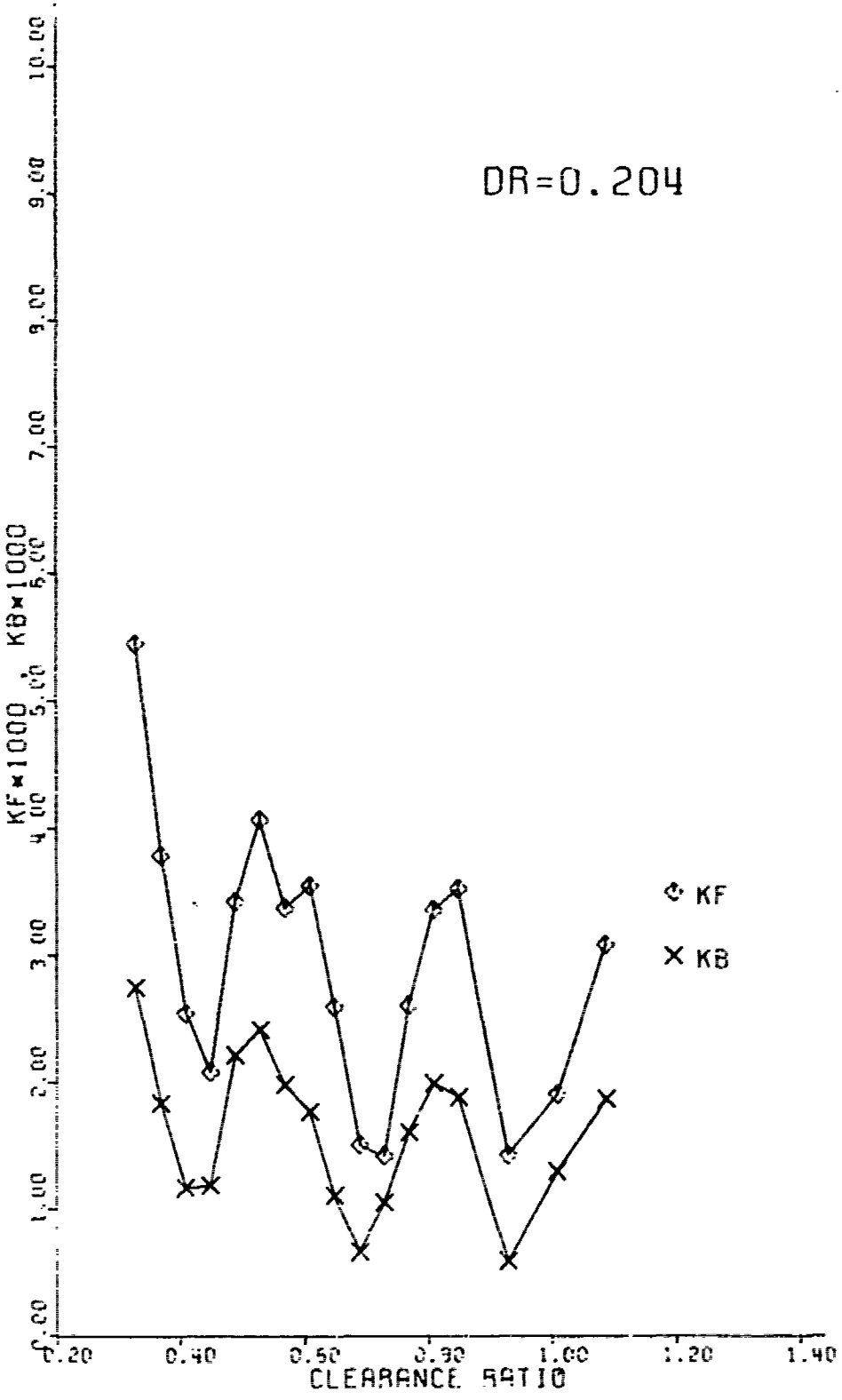

Fig. 8 : Rudder vibratory loading versus clearance ratio, DR=0.204

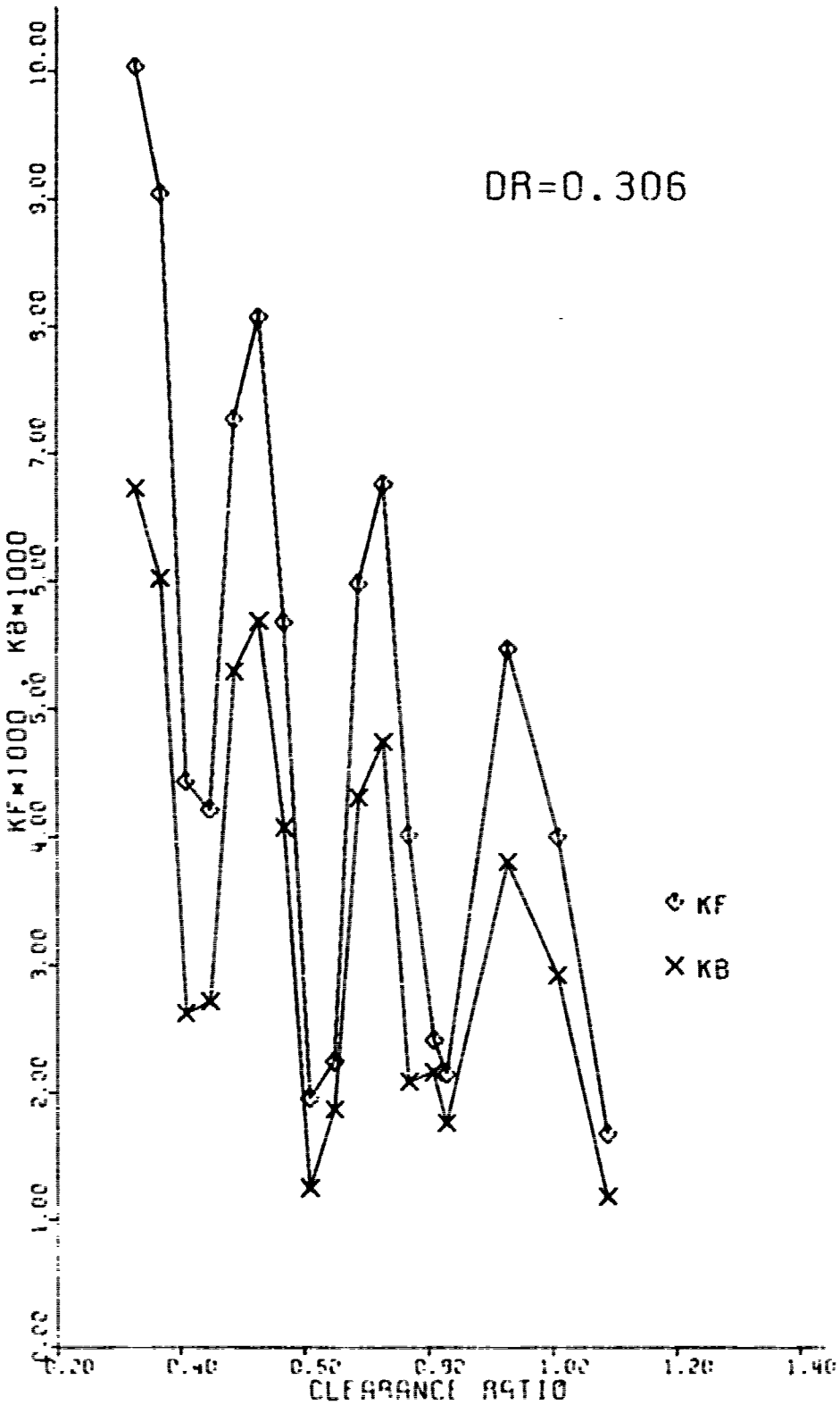

Fig. 9 : Rudder vibratory loading versus clearance ratio, DR=0.306

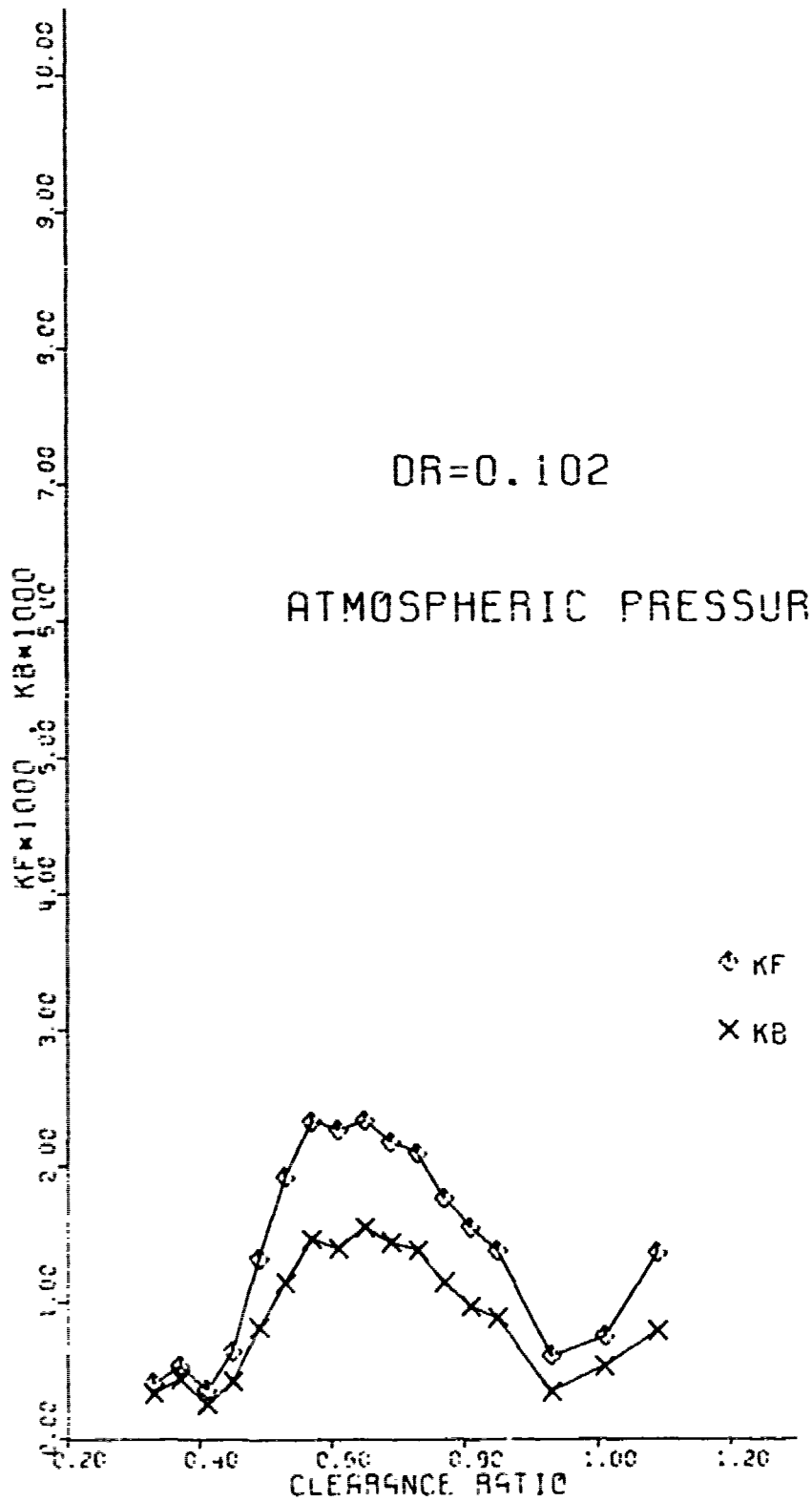

Fig. 10: Rudder vibratory loading versus clearance ratio, DR = 0.102, at atmospheric pressure.

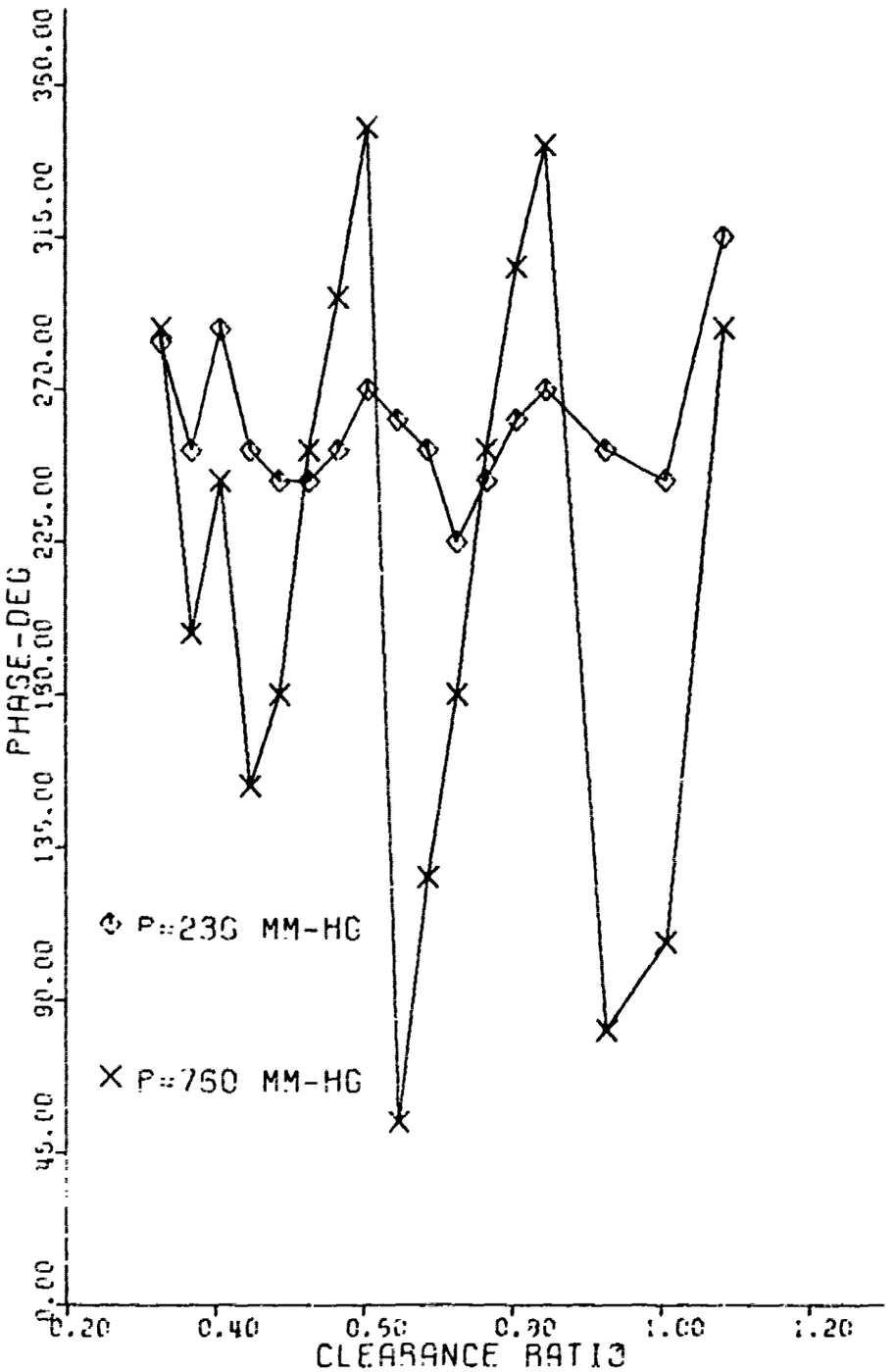

Fig.11: Phase angle measurements versus clearance ratio at two static pressures.

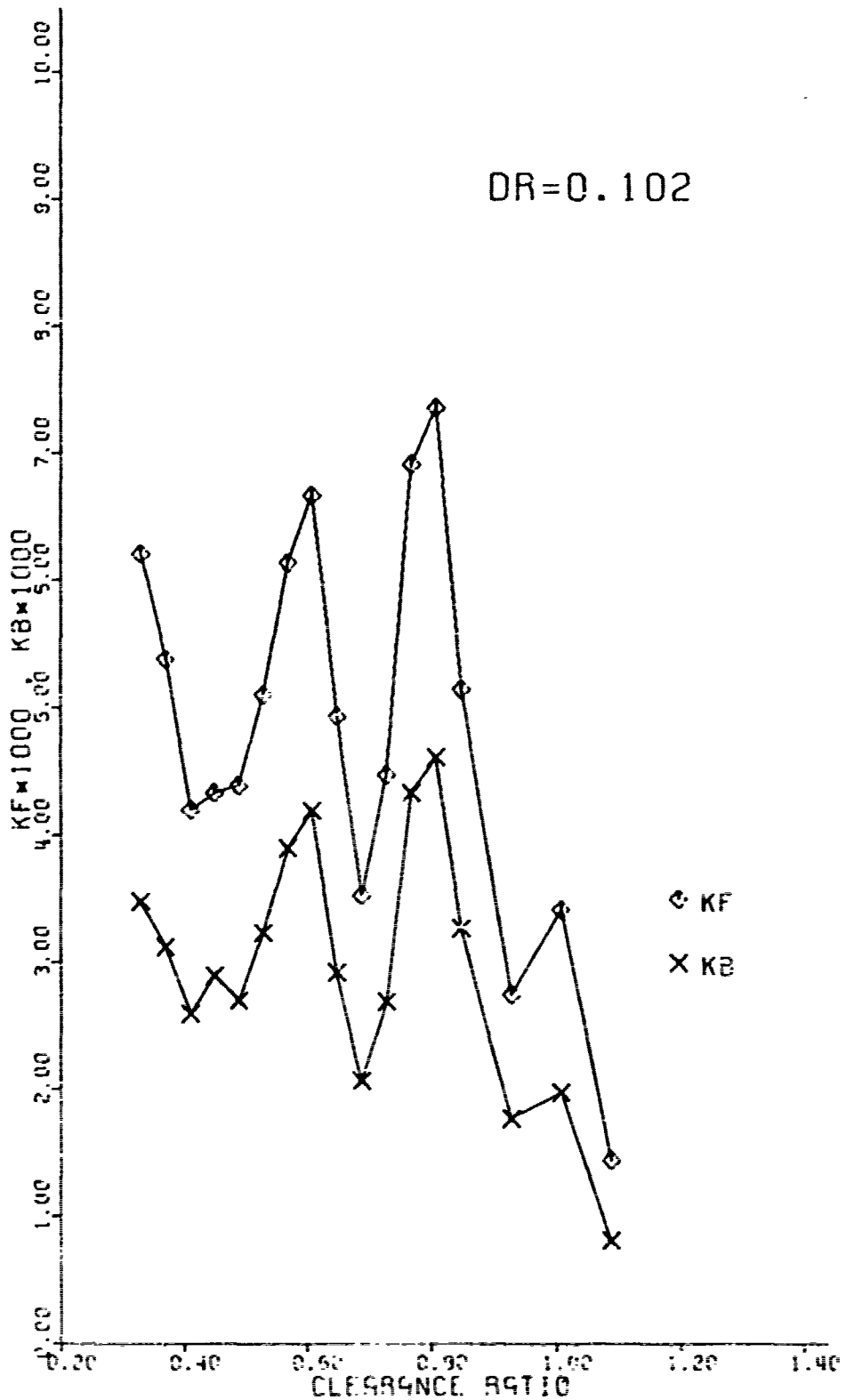

Fig.12: Rudder vibratory loading versus clearance ratio, DR = 0.102, high air-content in the tunnel water.

Fig.13: Photograph of propeller in test section during test

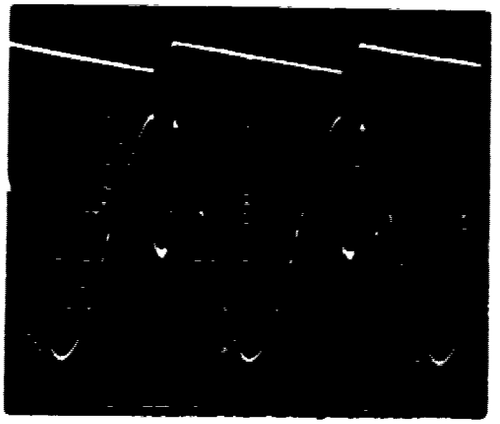

CR = .33

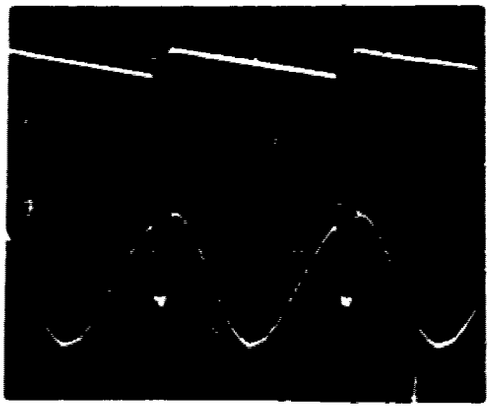

CR = .41

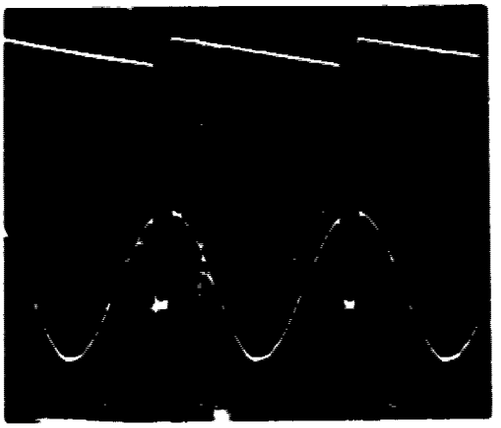

CR = .57

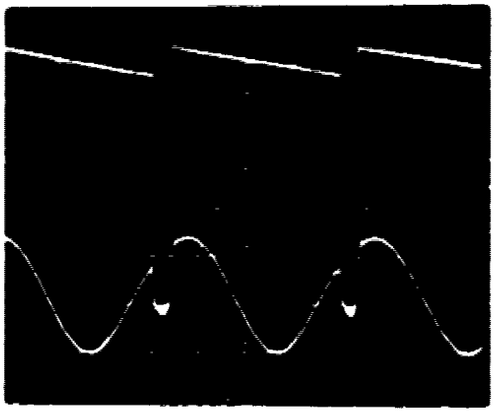

CR = 1.09

Fig.14: Photograph of the oscilloscope display of the Eductor output signal at four different clearance ratios.

ACKNOWLEDGEMENTS

The principal portion of the text of this report has been adapted from the Master of Science thesis of the same title completed by Anthony B. Zolotas in December, 1974.

The authors wish to acknowledge the major contribution of S. Dean Lewis, Senior Research Engineer at the MIT variable Pressure Water Tunnel, towards the design and development of the experimental apparatus. Thanks are also due to Professor F. M. Lewis, who first discovered the importance of optimum rudder orientation, Joseph Paglia of the Charles Stark Draper Laboratory, and Raymond Johnson and his assistants in the Mechanical Engineering Machine Shop who built most of the components of the model. Finally, we wish to thank technicians Harry McCall and Eddie Alcindor and graduate student Bohdan Oppenheim for their assistance in the conduct of the experiments.

6. REFERENCES

1) McGoldrick, R.T., "Ship Vibration," D.T.M.B.- Report 1451.

2) Lewis, F.M., "Propeller-Vibration Forces", Trans.S.N.A.M.E., 1963.

3) Lewis, F.M., "Propeller-Vibration Forces in Single-Screw Ships", Trans.S.N.A.M.E., 1969.

4) Sugai, K. "On Vibratory Forces Induced on the Rudder Behind a Propeller", Eleventh International Towing Tank Conference, The Society of Naval Architects of Japan, Tokyo, 1966.

5) Lehman, A.F. and Romandetto, R., "An Experimental Study of the Unsteady Forces Induced on a Rudder Due to a Propeller Acting in a Wake." Oceanics,Inc, Report 64-11, January 1964.

6) Lewis, F.M., "Propeller Excited Hull and Rudder Force Measurements" M.I.T. Report 73-10, April 1973.

7) McGoldrick, R.T., "Rudder-Excited Hull Vibration on USS Forrest Sherman", Trans.S.N.A.M.E.,1959.

8) Comstock, J.P.,Ed, Principles of Naval Architecture , S.N.A.M.E. 1967.

9) Oppenheim,B.W., "A Theoretical and Experimental Investigation of the Performance of Flapped Rudders", M.I.T.Thesis, 1974.

10) DenHartog,J.F., Mechanical Vibration, McGraw Hill Company, New York.

11) Burke, D.V.,"Discrete Vortex Theory for Propeller Non-Uniform Flow", M.I.T.Thesis, 1972.

12) Pfister, W.C., "Development of a Procedure to Measure Unsteady Propeller Forces", M.I.T. Thesis, 1971.

References (con'd)

13) Horton, C.O., "Design and Construction of a System Measurement of Unsteady Propeller Forces", M.I.T. Thesis, 1970

14) Glauert, H. Airfoil and Airscrew Theory, Cambridge University Press.

15) Eshbach, O.W., Ed., Handbook of Engineering Fundamertals, Wiley Handbook Series.

APPENDIX I

Testing Facilities and Resulting Design Considerations

The various tests to be described were conducted in the M.I.T. variable pressure water tunnel. The tunnel is of the closed circuit type having a test cross-section of 20 inches square and is capable of providing water speeds of about 10m/sec (33ft/sec) and can operate at pressures varying from atmospheric (760mm Hg) to about 100mm Hg.

All this information is relevant since it provides additional restrictions to the degree of simulation which can be achieved in the experiment.

Considerations such as tunnel wall interference and longitudinal travel of the propeller drive had to be investigated at this stage and the following decisions were made.

The transverse positions of rudder to be examined were to be restricted to 3 inches each way of the centre line at 1 inch intervals. This would provide sufficient points to enable us to reach acceptable conclusions. This decision was taken to satisfy the wall interference considerations as well as practical design problems which would have arisen otherwise.

Longitudinally, the restriction is imposed only in the aft movement of the rudder. In fact, it was decided that it would be much more simple to move the propeller longitudinally relative to the rudder, rather than the other way around. This is true because the tunnel is built to make provision for longitudinal movement of the propeller. Thus, although there is a physical limit to the length of travel of the drive shaft in the tunnel, it is such that it did not interfere with any of the positions we wanted to examine. Quarter inch spacing near the design location and half inch

intervals farther away, were found to be more than adequate.

An additional provision was also to be made in the design of the rudder mounting. This was to allow for variation of angle of attack of the rudder, 30° each way at 5° intervals.

Finally, we were to try to test at as high a propeller r.p.m. as possible. This would enable us to operate at high Reynold's numbers and, hence, reduce the scale effect on both propeller and rudder. It has also been noticed that better results are obtained when the tunnel is operated at higher pressures.

Natural Frequency Problems

About 30 different mounting configurations were examined in order to determine which one provided the "best" natural frequency characteristics on the rudder. One should note, however, that none of these bore all the features required for the final design, since, at that time, we were only interested in dynamic properties.

The experimental determination of the natural frequency of each configuration was quite simple. Essentially, the method used was the same as for the dynamic calibration (see Appendix IV) with the difference that the frequency of excitation was varied to scan the entire range of feasible operating values (0-300 Hz). Since we were not interested in quantitative results, the output signal from the sensor was fed into an ordinary oscilloscope where amplitude peaks could easily be seen.

In conjunction with the experimental investigation of the system's dynamic properties, attempts were made to use a theoretical approach to check the results. Most of these attempts, however, failed. The number of approximations as well as the fact that in most cases the boundary

conditions were ill defined, lead to results which were seldom verified experimentally.

The experience gathered from the various tests can be summarized as follows:

1) The natural frequency of the system was considerably increased when the dynamometer was clamped tight at more than one location, one of which was as close to the rudder as possible.

2) In most cases an increase in the mass on which the clamp was attached raised the natural frequency (not considerably however).

3) An increase in damping would almost always result in a drop in the peak response of the system although this would also increase the spread of the peak. The degree to which the natural frequency would be affected by damping was very much dependent on the overall configuration.

4) The window boundary conditions can have little or great effect on the dynamic properties of the entire system depending on the way the dynamometer is held.

Unfortunately, this piece of valuable information was not perceived until the final design was built. Most of the testing until then had been carried out with the window sitting on a bench rather than the tunnel. This was decided after our first few sets of results obtained on the tunnel were duplicated on the bench.

Bearing in mind (1), (2), and (3) above and ignoring (4) we went on and built our apparatus, an assembly of which is shown in fig.1. The effect of the window's boundary conditions showed up immediately after the first test. The natural frequency of the window just resting on top of the tunnel was 210 Hz (not far from what we were expecting).

However, as soon as the window was bolted down tight, the same natural frequency dropped to 93Hz. Unfortunately, to avoid leakage through the window sides, it was in this latter way that the experiment had to be carried out. One should note that both values quoted above were for tests in air. In water the"added mass effect" reduced these values even further.

This sudden drop in the first natural frequency, it was later decided, was due to the entire rig vibrating on top of the window about a horizontal axis passing through the centre of the plate (see fig.1). This mode of vibration was present only when the window was constrained so as not to move on the tunnel. The second natural frequency, however, was due to the 2-noded flexural vibration of the sensor-rudder subassembly acting as a very flexible cantilevered beam carrying a heavy mass at its end.

Thus our original aim of operating at a frequency below the first natural had to be abandoned and we had to live with the fact that we had to operate between the first and second modes.

Operating between two natural frequencies is frequently avoided because of instabilities in amplitude and mainly phase which may occur in the output response. Having established, however, that the first natural frequency was not due to the rudder-sensor subassembly but rather due to the entire rig, we anticipated little variation in either amplitude or phase provided the distance between the two peaks was sufficiently large.

To ensure an even larger spacing, we decided to lower the stiffness of the system by soft mounting the steel plates onto the window.

This decision was proved correct. When we scanned the range of possible operating frequencies we observed that the first natural frequency had dropped to 76Hz (in water) whilst the second had been pushed up to 275 Hz.

We also discovered that between 120 and 200 Hz there existed a band in which neither amplitude nor phase appeared to change at all.

Additional tests, using a ubiquitous spectrum analyzer (FEDERAL SCIENTIFIC MODEL VA-15A), to scan the frequencies between these two values made us decide to fix our operating blade frequency for the experiment at 125 Hz which corresponds to a shaft frequency, N, equal to 1500 R.P.M.

Having fixed one of the tunnel operating parameters, dynamic similarity considerations immediately determine the remaining two, namely water speed, V_T, and static pressure, P_{ST} (see Appendix V). From fig.(22) and (23) we see that the resulting final values of these two parameters are 17.3 ft/sec and 236mmHg respectively.

APPENDIX II

The Six Component Dynamometer

The six degrees of freedom dynamometer was designed and built between 1969 and 1970, as part of a project sponsored by the National Science Foundation. Its original purpose was to measure unsteady forces and moments on a propeller. A description of the sensor and the strain guages' mounting and wiring is given in great detail in refs. (11-13) and is beyond the scope of this report.

It is, however, necessary to outline the few alterations on the original design that had to be made to enable its use as a rudder dynamometer capable of measuring both steady and vibratory loads. A couple more points relevant to this experiment are also brought up for the benefit of similar tests in the future.

The most important modification on the original design was the introduction of potentiometers in the amplifier circuits. These are essentially, additional sources of input to the amplifiers which can be controlled externally and can be used to alter the net amplifier output voltage. With their addition, the no-load input voltage can be biased in such a way so that when loads are applied, the net output voltage will be below the amplifier's saturation value. Therefore, depending on the value of the potentiometer resistors, the span of the possible voltages which may be obtained from the amplifier, can be increased to as much as twice the value without the potentiometers.

At present, the potentiometers for each strain gauge bridge are capable of causing, at minimum gain, the bias shown on the table below. Clearly, voltages greater than 15 + |bias| will always saturate the amplifier (this was frequently the case when the rudder angle of attack was greater than 5°); it should also be noted that the higher the amplifier gain the smaller the voltage needed to cause saturation. A schematic of the strain gauge bridge circuit is shown in fig.(15).

BRIDGE	F_x	F_z	B_x	B_z	F_y	B_y
BIAS	±14.7	±11.0	±4.6	±4.6	±17.7	±2.7

The amount of bias which can be achieved by the individual potentiometers can be further increased by reducing the value of R_b. There is, however, no easy access to this resistor so that whenever possible such a change should be left as a last resort.

Lowering the amplifier gain is another way of avoiding saturation. This is a function of the ratio R_{AB}/R_{BC} and the feedback network resistor R_F. A reduction in either of these quantities will result in lowering the gain. The easier one to reduce is R_{AB} by simply adding another resistor R_g across the terminals 1 and 2 (see fig. 15). The minimum gain which can be achieved in this way is 1/10 of the original value. Further reductions in gain are much harder to accomplish and require, a major overhaul of the dynamometer.

To prevent damage to the circuitry the strain gauges had to be carefully waterproofed (previous experiments, using this dynamometer, had failed

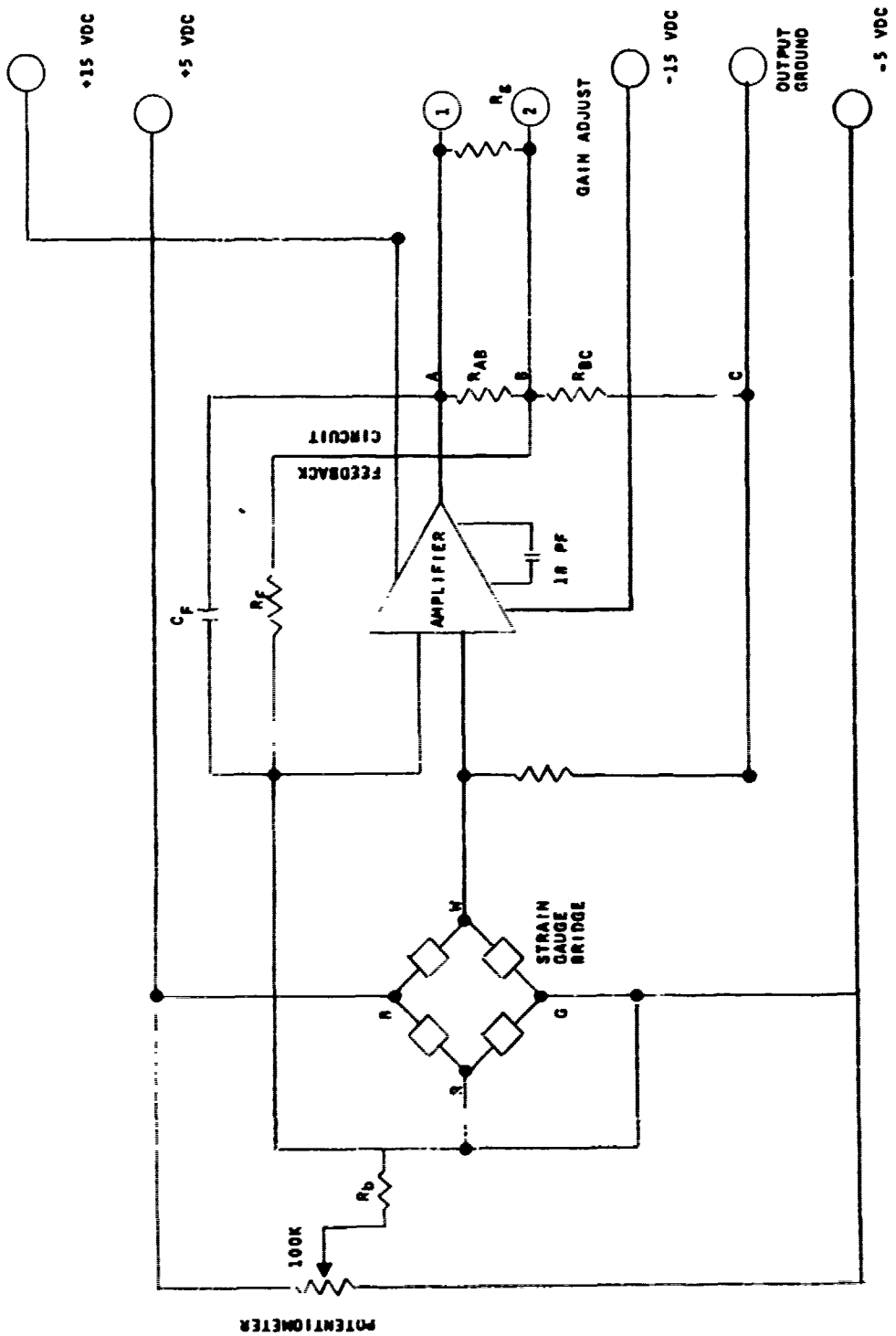

Fig.15: Typical dynamometer strain gauge circuit

because of unsuccessful waterproofing). This was accomplished by lowering the bottom part of the sensor into molten bee's wax until a thick protective layer was built up on the gauges. Excess wax was machined off on a lathe. The wax itself was coated with a layer of M-COAT G resin (M-LINE ACCESSORIES) which although it proved out to adhere poorly on either wax or steel, it nevertheless provided some additional shock protection of the gauges. The dynamometer before and after waterproofing can be seen in fig.(16).

Some additional wax was used to fill part of the core of the dynamometer. This was done in appreciation of the fact that the reduced pressure in the tunnel could force air bubbles through the small holes on the dynamometer wall (in the proximity of the gauges) into the protective layer of wax, thus damaging the waterproofing.

Finally, since the dynamometer was now used to measure forces and moments on a rudder the propeller based coordinate system was no longer valid. As a result, the various strain gauge bridges, channels, etc. had to be relabelled in a manner consistent with previous rudder tests. The "new" coordinate system adopted is the universally accepted rudder right-handed system (see fig.(17)).

The Waveform Eductor

The PRINCETON APPLIED RESEARCH Waveform Eductor makes use of the fact that the mean value of any single point on a signal consisting of a repetitive waveform plus non-synchronous signals and random noise is simply the point value of the repetitive waveform itself. As a result what it essentially does is to sample consecutively the signal input over 100 equal intervals each

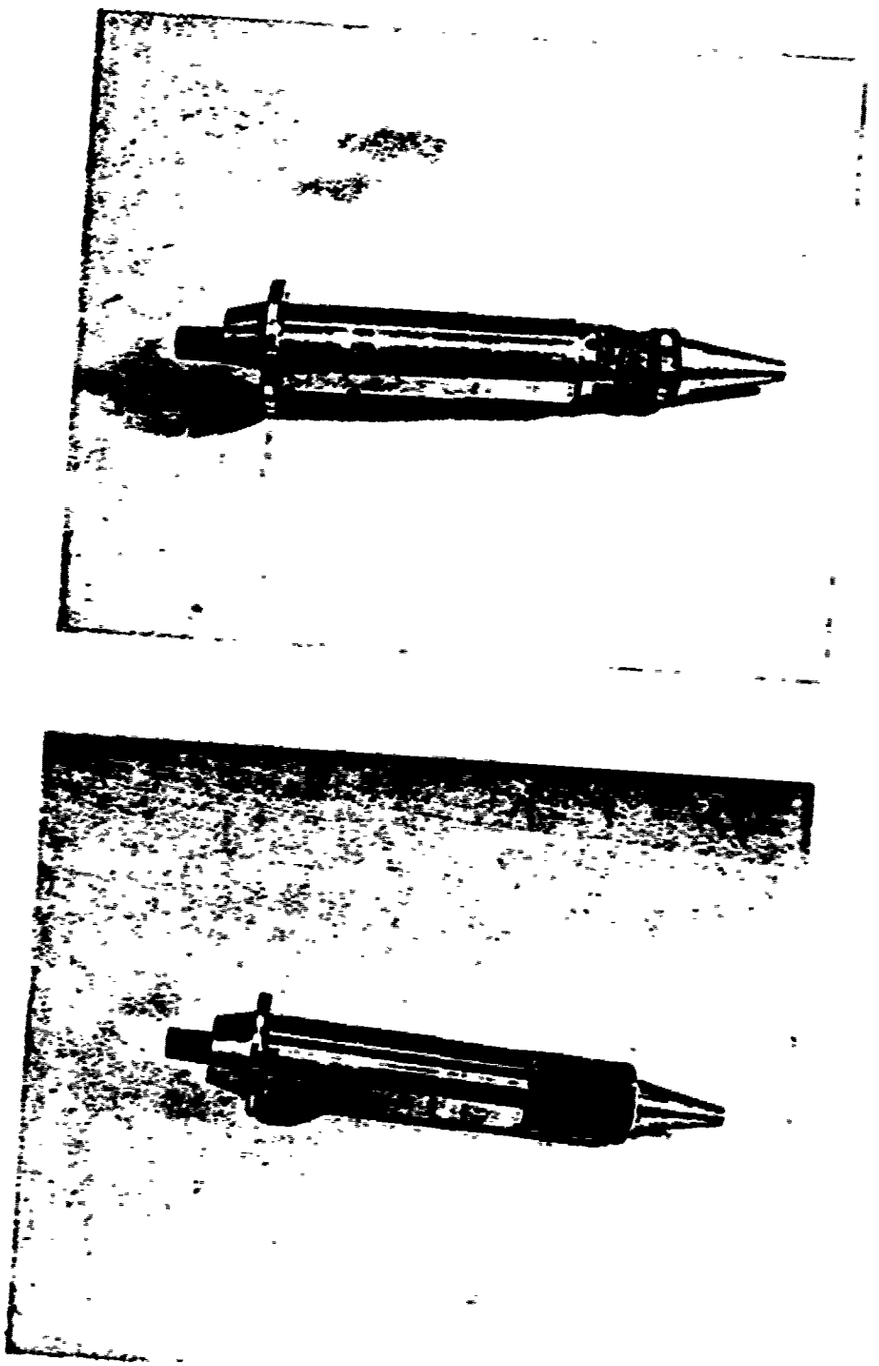

Fig.16: Dynamometer before and after waterproofing of strain gauge circuitry.

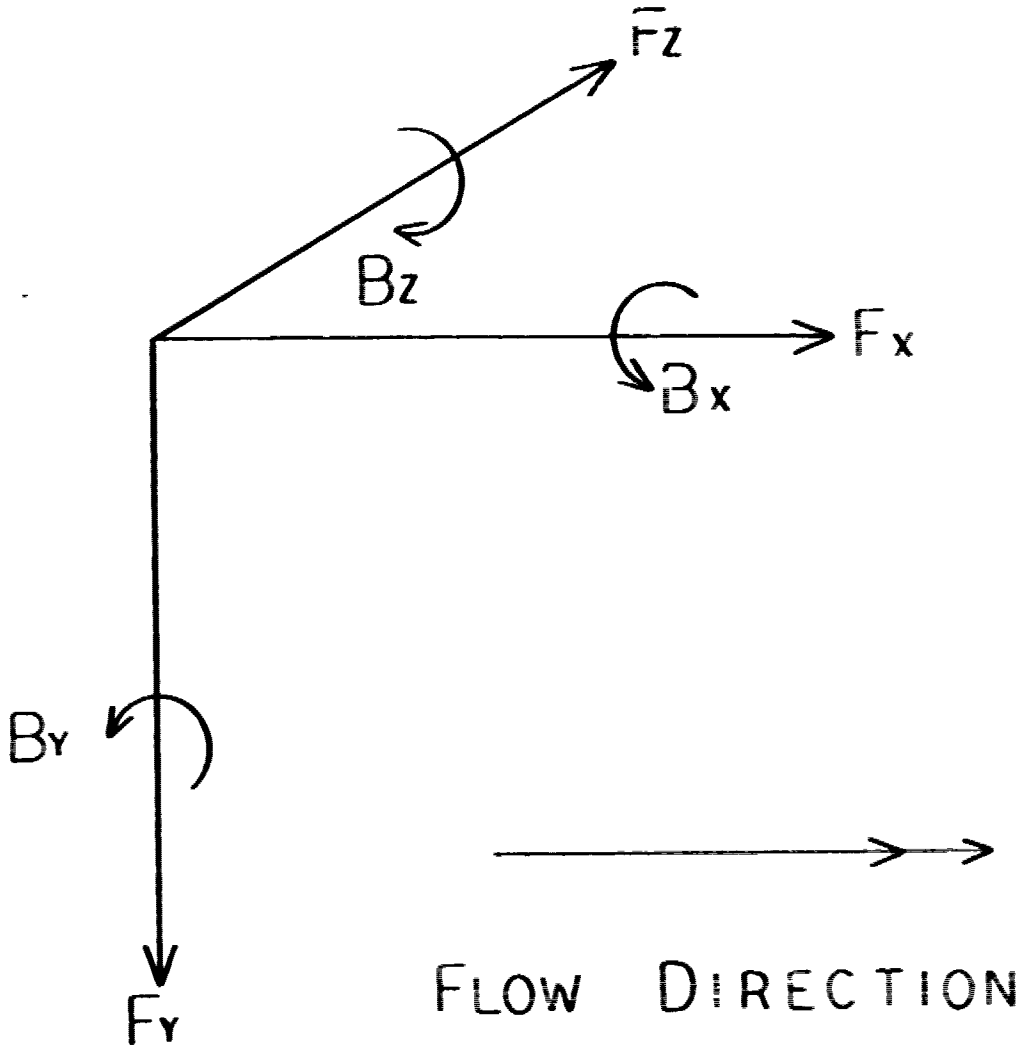

Fig.17: Rudder dynamometer coordinate systems

time the repetitive waveform occurs, separately integrating to suppress the noise, and finally storing each integrated sample in its memory. With each sweep the contents of the memory are reviewed and asymptotically approach the point by point value of the repetitive part of the signal even though at the input the repetitive part of the signal might have been completely buried in noise.

Synchronizing the sweep with the external event can be achieved by supplying a trigger pulse to the Eductor either automatically (externally or internally) or manually. (Since in the experiment to be described external triggering was used there is no need at this point to elaborate any further on the other triggering methods.)

An important feature of the Eductor is that it allows the user to choose both the *sweep duration* and the instrument's *characteristic time constant*. In fact these quantities are interrelated and it is possible by combining them in a proper way to optimize the efficiency of a run. The importance of this feature is evident when one considers the number of points that had to be investigated in each run.

By sweep duration one means that fraction of the *sweep period* (or time between two consecutive triggering spikes) the machine examines the input signal and adds information to its memory. For efficient runs one should arrange so that the sweep duration is just less than the sweep period. The reason behind this can best be illustrated by considering the following

For a 5-bladed propeller the period of the repetitive waveform is given by (1/blade frequency) and is essentially the time it takes for one blade to cover 1/5 of a revolution (i.e. 72°). For a blade frequency of

125Hz this period is thus 8msecs. Assuming now that we are interested in viewing only one period of this wave, (i.e. we want the sweep period to be equal to the waveform period). If the sweep duration is set to 7.8msecs, say, the Eductor will be adding to its memory over 97% of the signal duration having to wait for only 2msecs for the next trigger. On the scope the signal will look as on fig.(18) case a.

Had the sweep duration been a fraction larger than the waveform period, 8.2msecs say, then the Eductor would miss completely one triggering spike taking, thus, twice as much time to extract the complete signal. On the scope the signal would now look as on fig.(18) case b. Another reason why the sweep duration in case a should be preferred to the one in case b is strictly qualitative. It is essentially due to the fact that during "off" time there is a tendency for significant quantities of charge to leak off the memory capacitors and correspondingly a greater likelihood of distortion in the stored waveform. It is evident that in the second case the "off" time of the instrument is greater.

The ratio (sweep duration/sweep period) is known as the duty factor (D.F.) and its knowledge is important in estimating the real time required to charge the memory to within 1% of the applied voltage.

The characteristic time constant (τ) determines directly the time required for the Eductor to store the repetitive waveform component of the input signal in its memory. One should note, however, that this time is actual instrument integrating (or sweeping) time and differs from the real or "clock time" by the duty factor.

The instrument's active time required to charge the memory to 1% of

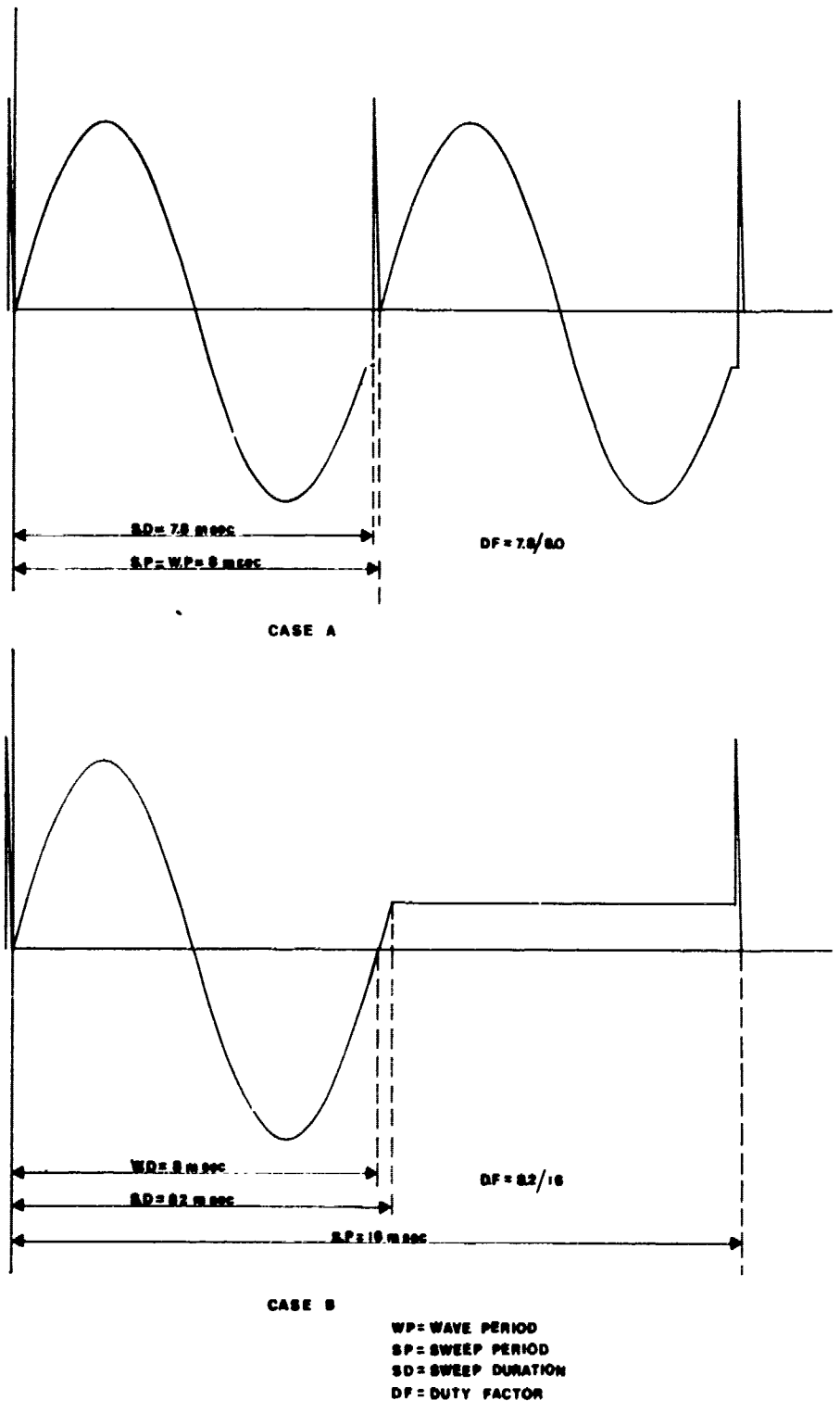

Fig.18: Typical effects on the Eductor output signal due to changing "sweep duration"

the applied voltage is $5\times\tau$. Therefore, real time is given by

$$\text{Real Time} = \frac{5\times\tau}{\text{D.F.}}$$

In choosing the operating value of τ one should give equal consideration to both the efficiency of the run and to the fact that increasing τ gives a slightly better resolution. For example, for a signal with large noise to signal ratio a larger value of τ should be preferred even though this may penalize the efficiency. An idea of how to pick an "optimum" value of τ may be taken from the instrument's operating manual where τ is plotted vs. D.F., sweep duration and noise to signal ratio.

Measurement of the Model Testing Parameters

Having already decided on the final values of the operating parameters N, V_T, and P_{st} it is worth mentioning the way they were measured in the tunnel.

Shaft frequency is measured by means of a magnetic pick-up sending out pulses, everytime a tooth of a 60-tooth gear passes underneath it. This gear which rotates with a shaft, comes as part of the propeller thrust and torque transducer package, located at the rear end of the tunnel. The number of pulses thus generated is measured by an electronic counter (HP model 5321B) over a given period of time which for the particular case was set to one second. Clearly the number of pulses per second received by the counter corresponds to the shaft frequency measured in r.p.m.

Water speed can be determined from the difference in the pressures

obtained at two points located at the entry to the test section. This pressure difference, in this particular test, was measured on a 3 yard long differential manometer which uses "blue fluid" as the working fluid instead of mercury. This last decision was made in anticipation of the fact that, in order to increase the sensitivity of the manometer readings, a low specific gravity fluid should be used. The fluid chosen (MERIAM D-8325 indicator fluid) is considerably less dense than mercury, having a specific gravity of 1.75 at 55°F. The relationship between the height of the "blue fluid" column, H_b, and the water speed at the entry to the test section, V, is given by

$$H_b = 4.11 \times C' \times V^{2.026} \qquad (1)$$

where C' is a temperature correction factor.

In our case, however, the desired water speed of 17.3 ft/sec is the value at the middle of the test section which due to the presence of the splitter plate and the resulting decrease in cross sectional area, is different from the value at the entry. Measurements with a pitot static probe indicated that the former value was 1.091 × V so that equation (1) above can be rewritten as

$$H_b = 4.11 \times C' \times (V_T/1.091)^{2.026} \qquad (2)$$

Substituting 17.31 ft/sec for V_T and 1.35264 for C' we get from (2) that the value of H_b corresponds to the speed in the middle of the test

section is 1506mm.

Finally, static pressure at the centreline of the propeller is measured at two points, one at the entry and the other one at the exit of the test section. The two pressures transmitted through tubes are averaged at a merging point, and the resulting mean value is read on a mercury manometer (reading absolute rather than gauge pressure).

APPENDIX III

Water Tunnel Wake Survey

To achieve an even higher degree of simulation it was decided to reproduce in the tunnel the variable wake obtained behind the ship. Such a wake can be generated by inserting at the entrance to the test section a screen of variable solidity capable of creating a velocity profile having a variation in the axial velocity component.

The wake behind the ship was investigated in a wake survey carried out on a model in a towing tank. The results of this wake survey were given to us as ratios of the axial velocity of the flow behind the ship to the average free stream velocity, plotted against angular position at 4 different radial distances from the propeller shaft centreline.

From these results we were able to make the following observations:

1) A significant reduction of the axial velocity component was evident at all radii and at angles varying from +20 to -20 degrees to the upward vertical. This reduction, caused by potential flow pressure gradient interacting with hull viscosity effects as well as the pressure of the propeller shaft the axis of which was inclined relative to the flow, was more pronounced at the smaller radii.

2) At all radii there existed a transition zone between angles of ±20-35° where the flow was evidently affected by the presence of the vee-strut.

3) At the largest radius, 1.174×propeller radius the flow did not appear to recover from this transition zone, until the angle reached ±60°. This fact and close inspection of the ship's drawings suggested that at such a

large radius the proximity of the hull is a critical factor.

4) At large angles the longitudinal velocity-component ratio appeared to be fairly constant for all radii.

In the tunnel matching the wake of the ship presented certain problems. Based upon the observations above, it was decided to build a screen which would essentially consist of a frame of trapezoidal shape (see fig.20) on which a wire mesh whose variable solidity was to be evaluated experimentally was welded (solidity being defined as blocked area, Ab, divided by total area, Ab + Ao, where Ab is the projected area of the screen elements and Ao that of the openings).

We thus started with a screen of given solidity (.272) and carried out a wake survey in the tunnel in which we measured the velocity distribution behind the screen at four radii (corresponding to the four radii used in the towing tank survey). The water speed was measured by means of a pitot static probe, attached to the propeller drive shaft and thus able to assume any angular position by merely moving the drive belts at the back of the tunnel (see fig.19). The angle obtained was read to the nearest degree on a protractor fixed at the end of the shaft.

At each radius the water speed was measured at several angles within the region influenced by the screen and the ratio of each of these values to the fully developed "free" stream velocity was computed. Finally, the average of all these ratios, at each radius, was obtained and compared to the one obtained in the towing tank survey.

Depending on the difference between the 2 averages, the solidity of the screen was either decreased by removing some of the wire, or increased

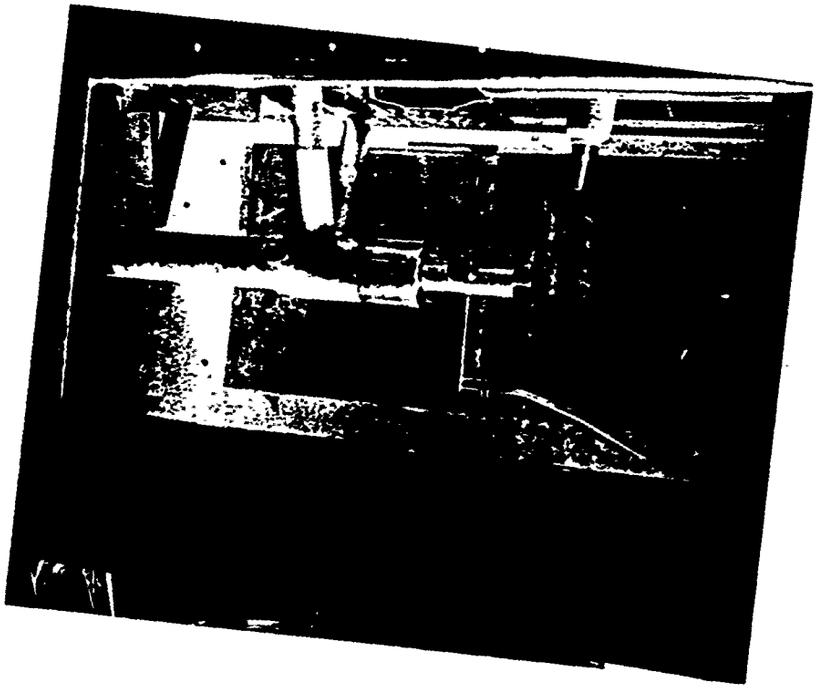

Fig.19: Photograph of test section arrangement during wake survey measurements.

by adding bits of wire mesh wherever necessary. This procedure was repeated until obtained and desired velocity distributions bore satisfactorily close resemblance.

The drawbacks of this method became apparent during the first test runs. Satisfying the high velocity requirements at certain radii meant reducing the solidity of the screen to a point where many and sometimes all of the transverse members of the mesh had to be removed. Besides weakening the screen as a whole, this meant that the remaining longitudinal wires were now free to deflect and reach larger curvatures than before with the result of being subjected to higher stresses.

This combined with the increase in the loading due to the reduction in pressure was sufficient to cause fatigue failure in a number of screen wires.

All this prompted us to find some other way of obtaining the required variable solidity and so we finally decided to handweave a screen on the frame. To do so we drilled a large number of closely spaced holes on all four sides of the frame through which long pieces of wire were weaved forming a mesh of longitudinal and transverse wires which now had considerably greater strength.

The first version of the screen was deliberately made less solid than what we anticipated the final version (after the wake survey) would be, to make sure that any changes would involve additions rather than removal of wire. The final version of the screen is shown on fig. (20).

The resulting wake behind the final screen bore a satisfactory resemblance with the wake obtained behind the model in the towing tank survey. The results of the two surveys are given in the following table (I).

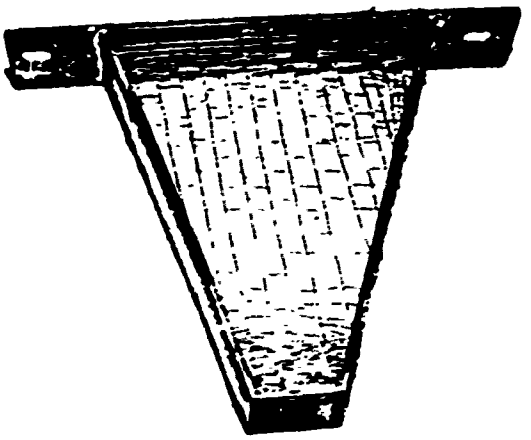

(a)

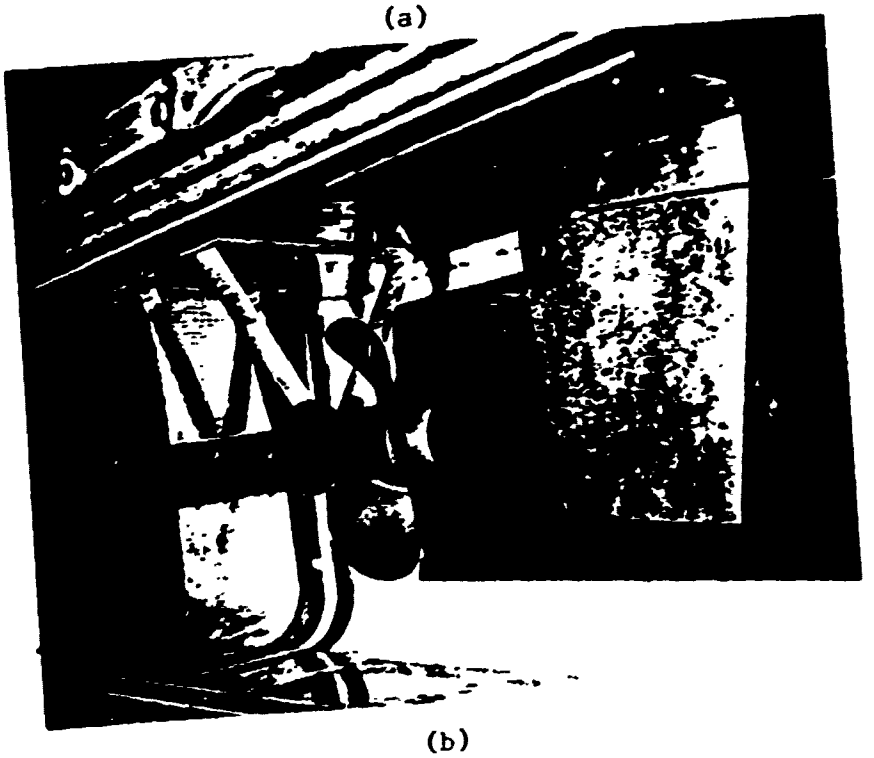

(b)

Fig.20: (a) Handwoven wake screen and (b) complete model scale simulation of ship configuration.

RADIUS	.357 × R	.555 × R	.772 × R	1.174 × R
TOWING TANK (SHIP'S MODEL)	$\frac{\overline{V}_x}{V} = .74$	$\frac{\overline{V}_x}{V} = .87$	$\frac{\overline{V}_x}{V} = .93$	$\frac{\overline{V}_x}{V} = .83$
WATER TUNNEL (WAKE SCREEN)	$\frac{\overline{V}_x}{V} = .78$	$\frac{\overline{V}_x}{V} = .86$	$\frac{\overline{V}_x}{V} = .93$	$\frac{\overline{V}_x}{V} = .835$

TABLE I : Average longitudinal velocity, $\overline{V}_x/V$, ratios at 4 radii as obtained in the towing tank and water tunnel wake surveys

Splitter Plate Boundary Layer

The introduction of the splitter plate, as already stated, was decided with 2 considerations in mind. Firstly, it was to serve the purpose of simulating the ship's hull by providing the proper propeller tip clearance. Secondly, it was hoped that by making it extend less upstream than the test section wall, the resulting boundary layer would be of smaller thickness than the one that would have developed on the wall otherwise.

For this, however, to be the case, it was established in previous experiments, that the leading edge had to be slightly curved upwards. The degree of this inclination was decided empirically based on the experience obtained with an earlier splitter plate used in the tunnel [9], whose 30° leading edge angle had managed to create a boundary layer of relatively small thickness.

Measuring the boundary layer thickness on the tunnel was relatively simple, involving a method quite similar to that used in the wake survey. The pitot static probe was raised until it almost touched the splitter plate at 0° to the vertical.. The water speed was measured at this radius and, as it was expected, was found to be very small . The probe was then rotated by small angular movements until a point was reached from which on the velocity read was constant. This point marked the end of the boundary layer. From the polar coordinates (r,θ) of this point one can evaluate the boundary layer thickness using the expression

$$\delta = r(1-\cos\theta) + h$$

where h is the 1/16 of an inch clearance between the probe at its upper-

most position and the splitter plate.

For $r = 7.5625$ inches and $\theta = 16°$ the boundary layer thickness was found to be .355 inches which is indeed a very satisfactory value. This result also happens to agree remarkably well with the one obtained if the following expression for a turbulent boundary layer on a flat plate is used

$$\delta = \frac{0.37x}{R^{1/5}}$$

where $R = \frac{Vd}{\nu}$ is the Reynolds' number

$x=d$ is the distance of the axis of rotation of the rudder from the leading edge of the splitter plate. (ft)

V is water speed (ft/sec).

ν is kinematic viscosity of water at 21°C ft^2/sec.

Substituting then in the above equation $V = 19.76$ ft/sec, $x=d=19/12$ ft and $\nu = 1.054\times10^{-5}$, we get that the boundary layer thickness on the plate should be .357 inches.

APPENDIX IV

Dynamic Calibration

As already stated, a dynamic calibration was carried out to determine the complex coefficients relating the true vibratory force and the moment (F_Z and B_X respectively) on the rudder to the output of the corresponding strain gauges.

A desired calibration force was produced by a known alternating current in a coil placed in the air gap of a permanent horseshoe shaped magnet and attached to the rudder at given locations.

The coil-magnet combination was first calibrated by measuring the steady force produced by a known direct current in the coil. The constant of the particular coil we used had been found by F.M. Lewis [6] to be .775 lbs/amp. Recalibration using a chemical scale with weights balancing out the steady magnetic force, yielded a constant equal to .75 lbs/amp. The difference between the two values was attributed to the fact that the magnet had been left for lengthy periods without its keeper with the result of losing part of the strength of its magnetic field.

The strain gauge calibration procedure was as follows. The coil was first bolted onto the rudder at some point Y_1 inches from the splitter plate (which was used as datum) as shown in fig. (21). With the magnet in position an alternating current from a signal generator (HP model 204C) of known frequency was passed through the coil via an amplifier (MC INTOSH model 200). The amplitude of the field current was determined by measuring V, the R.M.S. voltage drop across a 4.6Ω resistor placed in series with the

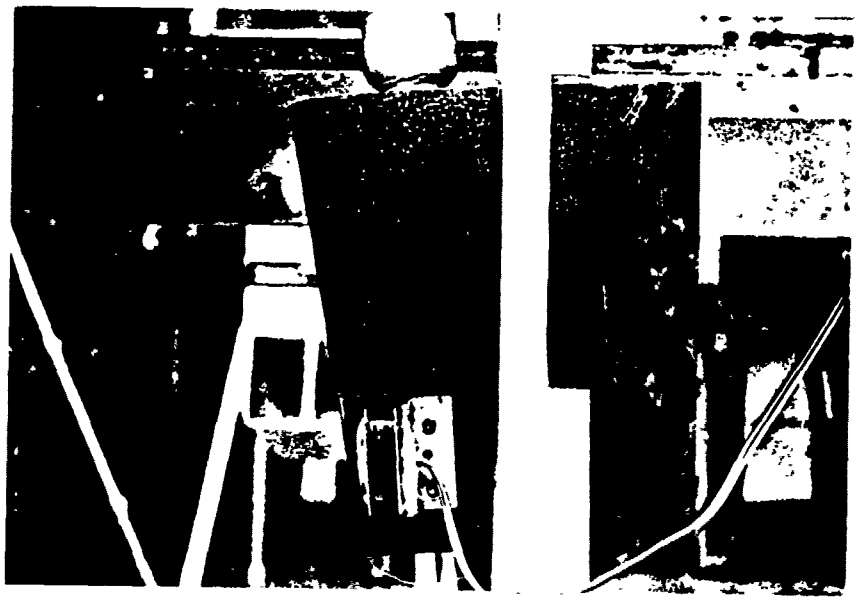

(a)

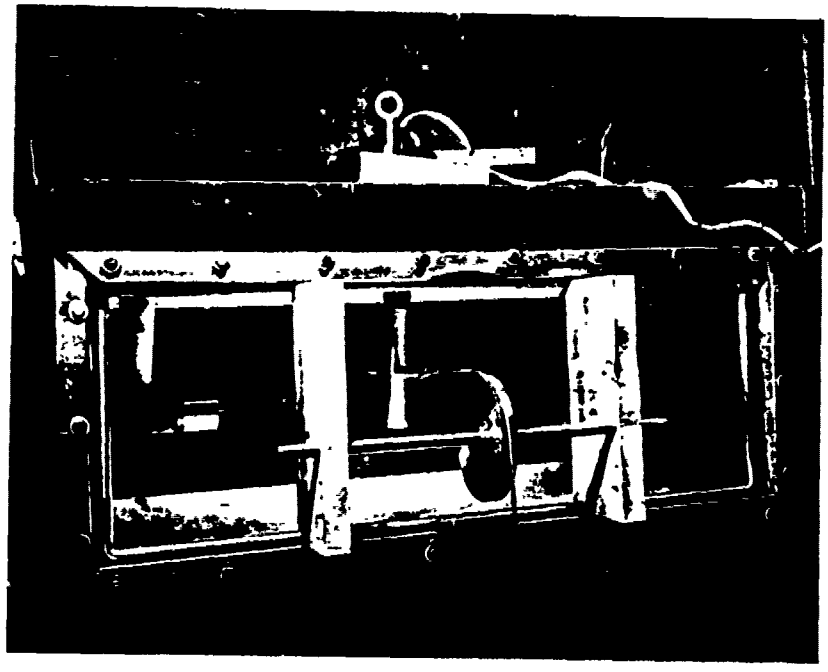

(b)

Fig.21: Photographs of (a) dynamic calibration rig and (b) static calibration rig.

coil. (V was measured with an HP vacuum tube voltmeter model 400D). Such an arrangement allowed the operator to keep the current input to the coil at a constant value independent of the exciting frequency.

The resulting peak force on the rudder was thus:

$$F_{CAL} \doteq \frac{\sqrt{2} \times .75 \times V}{4.6} \text{ lbs.}$$

The response of the strain gauges, F_{ZR} and B_{XR}, to this force was then fed through the waveform eductor onto an oscilloscope. A Polaroid picture of this output signal was then taken, on which the amplitude and phase were read.

This procedure was then repeated for another position of the coil, Y_2 inches from the splitter plate. Given the amplitude and phase of the sensor responses the *complex* coefficients, αij, can be evaluated from the following equations;

$$\text{at } Y_1 \qquad F_Z = F_{CAL} = \alpha_{11} F_{ZR1} + \alpha_{12} B_{XR1}$$

$$B_X = F_{CAL} \times Y_1 = \alpha_{21} F_{ZR1} + \alpha_{22} B_{XR1}$$

$$\text{at } Y_2 \qquad F_Z = F_{CAL} = \alpha_{11} F_{ZR2} + \alpha_{12} B_{XR2}$$

$$B_X = F_{CAL} \times Y_2 = \alpha_{21} F_{ZR2} + \alpha_{22} B_{XR2}$$

The solution of these four equations, which involves complex algebra, is carried out in the first part of the "dynamic data reduction program" (see Appendix VI).

Static Calibration

A static calibration of the sensor gauges was carried out to determine their response to steady loads. Although in theory it could have been carried

out in much the same way as the dynamic calibration (by passing a direct current through the coil) a different method was used. This was done in anticipation of the fact that during actual testing the steady loads acting on the rudder would be of a much greater order of magnitude than the ones that would possibly be applied through the coil.

The method used essentially consisted of hanging weights from a specially designed calibration rig bolted to the dynamometer in place of the rudder (fig.(21)). The rig makes provision for hanging weights from a number of different points at various distances from the gauges so that, depending on the point of application, a net force or a net moment may be applied. Since it was already decided that the vertically upward force on the rudder, F_v, was not to be measured, the corresponding channel was not calibrated.

Having a fairly good idea of the expected maximum values of the various loads we adjusted the amplifiers' gain accordingly by introducing resistances, R_g, across the terminals 1 and 2 of each bridge circuit (see fig.15). The values of these resistors and the resulting reduction in gain (as a fraction of maximum possible gain) is given below.

BRIDGE	F_x	F_z	B_x	B_z	B_y
RESISTOR R_g	4.64K	4.64K	shorted	3.32K	1.82K
GAIN	1/5	1/5	1/10	1/5	1/5

With the gain of each remaining channel adjusted to these final values the response of the strain gauges to various loads was read on a digital

indicator (LEBOW ASSOC. model 7521). As in the case of the dynamic calibration the net force (or moment) on the dynamometer in one direction was an algebraic combination of the readings of the force and moment channels in the same direction.

The results of the calibration, namely the matrix of the coefficients relating actual to read values, are shown below.

$$\begin{bmatrix} F_x \\ F_z \\ B_x \\ B_z \\ B_y \end{bmatrix} = \begin{bmatrix} -0.077 & 0 & 0 & -0.063 & 0 \\ 0 & 0.072 & 0.137 & 0 & 0 \\ 0 & -0.051 & 0.455 & 0 & 0 \\ -0.043 & 0 & 0 & 0.223 & 0 \\ 0 & 0 & 0 & 0 & -.65 \end{bmatrix} \begin{bmatrix} F_{xr} \\ F_{zr} \\ B_{xr} \\ B_{zr} \\ B_{yr} \end{bmatrix}$$

These results are used in the "steady state data reduction program" in the evaluation of the different forces and moments acting on the rudder (see Appendix VI).

APPENDIX V

Model to Ship Dynamic Similarity Considerations

In order for the results of the model experiments to be of any value to the actual ship, there are certain laws governing model to ship similitude which need to be obeyed. These laws are determined by making use of dimensional analysis.

If we apply dimensional analysis in examining the thrust on a propeller we come up with an equation for the thrust coefficient of the form

$$\frac{T}{\rho D^2 V_A^2} = f\left[\frac{gD}{V_A^2}, \frac{\nu}{V_A D}, \frac{nD}{V_A}, \frac{p}{\rho V_A^2}\right] = f\left[F_n, R_n, J, \sigma\right]$$

This equation states that for similar flow patterns and thrust coefficients for the model and the ship, the values of the non-dimensional groups on the right-hand side in the two cases must be the same.

Satisfying both the Froude number and the Reynolds number equality constraints is not possible. In water tunnel experiments, (as opposed to open water tests) it is common practice to satisfy the Reynolds number requirement, being prepared to accept differences in the local pressure distributions across the disk, for the benefit of avoiding more critical problems of scale effect. Thus, water tunnel experiments are run at high speeds and the friction scale effect is small. The two remaining requirements concerning similarity of advance coefficient, J, and cavitation number, σ, can easily be satisfied in the water tunnel as shown below.

In general, the cavitation number is defined as

$$\sigma = \frac{P_{static} - P_{vapour}}{1/2\rho V^2}$$

In the case of the ship, the expression above becomes

$$\sigma_s = \frac{P_{atm} - P_{hyd} - P_{vap}}{1/2\rho V_A 2}$$

where

P_{atm}	= atmospheric pressure	2116 lb/ft^2
P_{hyd}	= hydrostatic pressure = ρgh	
ρ	= salt water density	1.99 $slugs/ft^3$
g	= gravitational acceleration	32.2 ft/sec^2
h	= depth to propeller centreline	20 ft.
P_{vap}	= vapour pressure (from tables)	44.56 lb/ft^2
V_A	= advance speed = $(1-w_T) \times V_S$	
V_S	= ship speed	42.23 ft/sec
w_T	= Taylor's wake fraction	0.025

If we substitute all the above values in the equation for σ_s we get that for the particular ship

$$\sigma_s = 2.0$$

For the water tunnel the cavitation number expression becomes

$$\sigma_T = \frac{P_{st} - P_{vap}}{1/2\ \rho_T V_T 2} \quad \frac{1}{.3591}$$

where

P_{st} = static pressure (in mmHg)

P_{vap} = vapour pressure (from tables) 26mmHg

ρ_T = tunnel water density 1.93 slugs/ft^3

V_T = tunnel water speed (in ft/sec)

Equating the two cavitation numbers for the tunnel and the ship, we obtain a relationship between V_T and P_{st} in the form

$$P_{st} = \alpha V_T^2 + \beta \qquad (1)$$

where α and β are known constants.

A second equation can be obtained by equating the values for J for the ship and the model

$$J_T = J_S = \frac{V_T \times 60}{ND}$$

where

J_S = advance coefficient for the ship .85

D = model propeller diameter .8205ft.

J_T = advance coefficient for the model

N = model propeller r.p.m.

Thus we have a second relationship between the tunnel parameters in the form

$$V_T = \gamma N \qquad (2)$$

where γ is again a constant.

A graphical representation of equations (1) and (2) is given in fig. (22 and 23). Clearly, by choosing a value for N, values of V_T and P_{st} can immediately be obtained from these graphs. A limitation to the minimum value of V_T is imposed by the high Reynolds number requirement and so values below 11ft/sec are not very desirable. The final choice of tunnel operating parameters used in the experiment was based upon the natural frequency characteristics of the system as emphasized in Appendix I.

Water Tunnel Wall Interference Correction

Due to the presence of the boundary it is not possible to develop free stream flow in the tunnel. As a result, any information related to rudder characteristics obtained in the experiment must be corrected for wall interference, prior to being made applicable to the ship itself.

For a closed working section tunnel the condition that needs to be satisfied at the boundary is that the normal to the wall component of the velocity must be zero. This boundary condition can be satisfied analytically by the introduction of a suitable series of images of the model, the interference experienced being the induced velocity corresponding to the vortex system of these images [14].

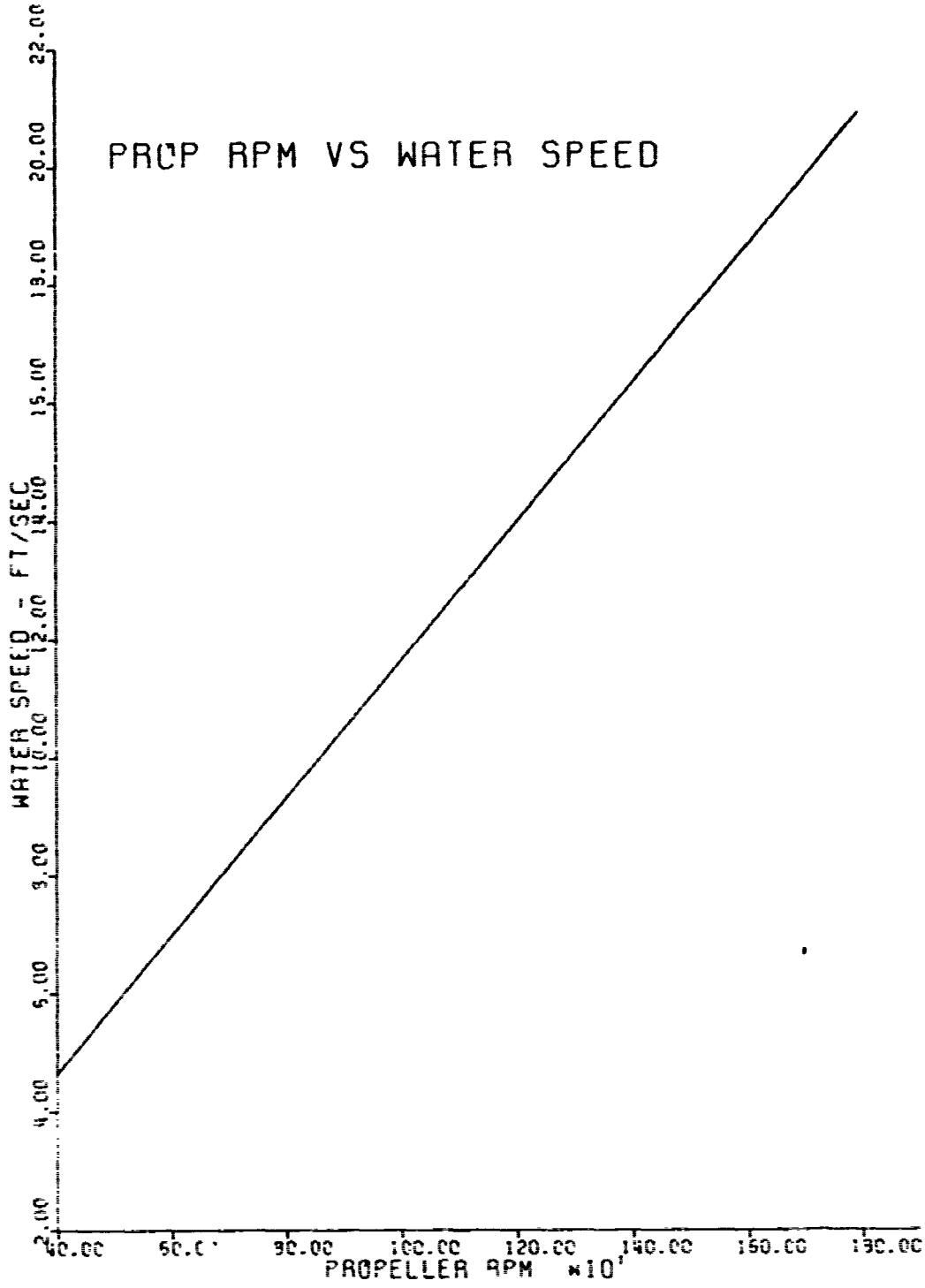

Fig.22: Propeller RPM versus tunnel water speed to simulate ship advance coefficient.

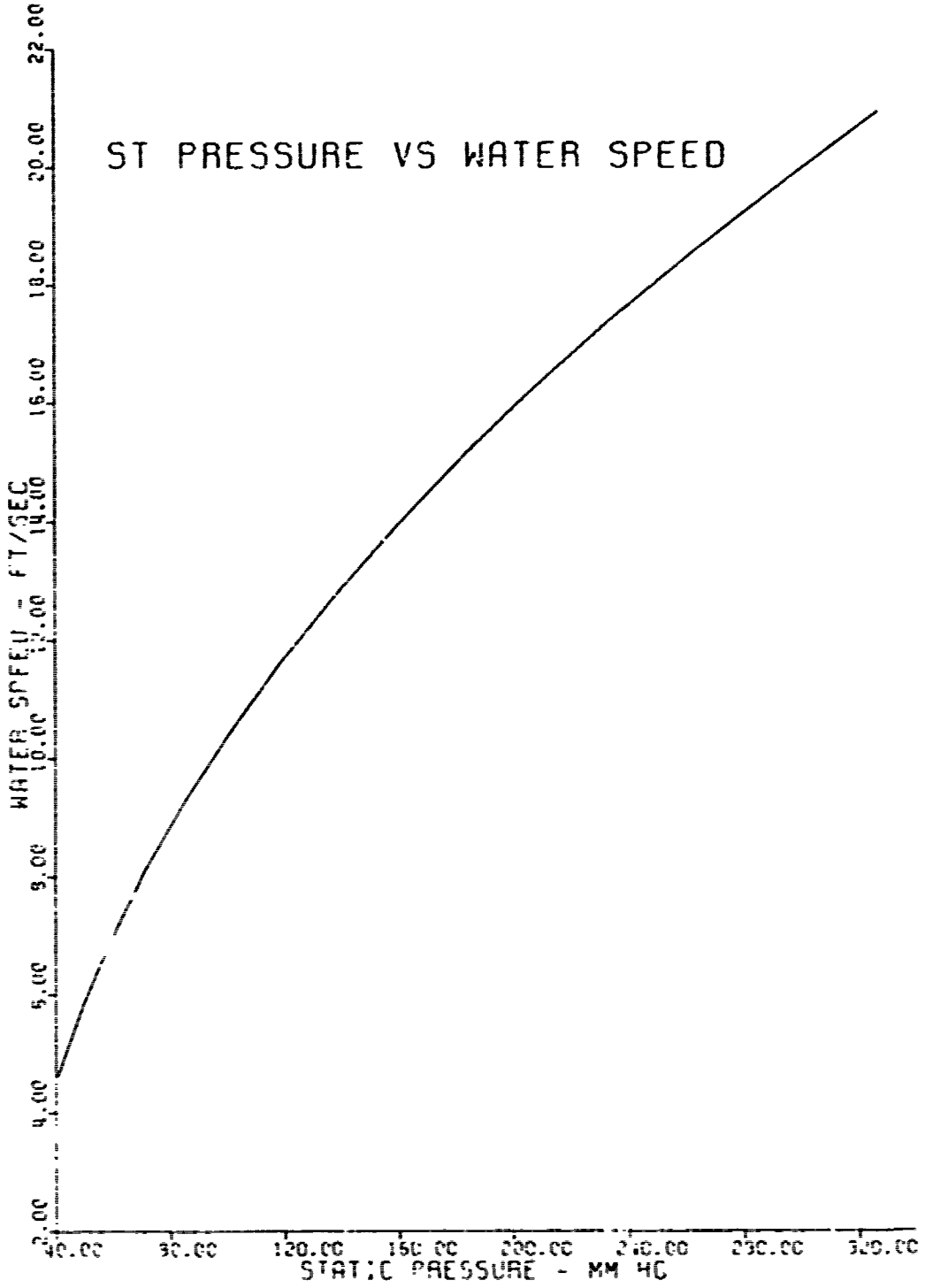

Fig.23: Static pressure versus tunnel water speed to simulate ship cavitation number.

In the case of a tunnel with rectangular cross section of breadth "b" and height "h" the upward inclination of the stream caused by the combined effect of the whole system of images is given by

$$\epsilon = \frac{S \times C_L}{8\pi b^2} \sum_{-\infty}^{\infty}\sum_{-\infty}^{\infty} (-1)^n \frac{m^2-\lambda^2 n^2}{(m^2+\lambda^2 n^2)^2} = \delta \times \frac{S}{C} \times C_L \qquad (1)$$

where λ = h/b

S = total wing area of model

C_L = lift coefficient

C = cross sectional area of the tunnel = b × h

but

$$\sum_{-\infty}^{\infty}\sum_{-\infty}^{\infty}(-1)^n \frac{m^2-\lambda^2 n^2}{(m^2+\lambda^2 n^2)^2} = \frac{\pi^2}{3} + 8\pi^2 \sum_{i=1}^{\infty} \frac{i}{1+e^{2\lambda\pi i}} = \phi$$

Sufficiently accurate results may be obtained by retaining only the first term of the last exponent series and, hence,

$$\phi = \frac{\pi^2}{3} + \frac{8\pi^2}{1+e^{2\lambda\pi}} \qquad (2)$$

And therefore,

$$\epsilon = \frac{S \times C_L}{8\pi b^2} \times \phi = \delta \times \frac{S}{C} \times C_L \qquad (3)$$

where

$$\delta = \phi \times \frac{h}{b} \times \frac{1}{8\pi} \qquad (4)$$

The drag coefficient C_D needs also to be corrected for wall interference

by ΔC_D given by

$$\Delta C_D = \varepsilon \times C_L = \delta \times \frac{S}{C} \times C_L^2 \qquad (5)$$

The corrections in both angle of incidence, ε, and drag coefficient, ΔC_D, are incorporated in the "steady state data reduction program". (see Appendix VI).

Data Reduction Computer Programs

1. Functional Description - Steady-State Data Reduction Program

This program accepts as input raw data recorded directly from the water tunnel instruments during a steady-state rudder performance test. The data are then converted to appropriate physical units which are then combined to produce the output non-dimensional coefficients. A detailed description of each segment of the program is as follows:

Lines	Function
150-190	Read input constants
	TWIST = Torsional stiffness of rudder shaft (used to correct angle of attack for deflection under load)
	SHAFT = Shaft diameter (used to correct vertical force for tunnel pressure difference; not used in this application)
	NRT,NTT = Room and tunnel temperature - deg. F.
	AREA = Rudder area
	SPAN = " span
	MAC = longitudinal position of mean aerodynamic center from rudder shaft
	AZL = Instrument zero reading for angle of attack
	VELINC = Velocity increment due to blockage effect of splitter plate
240-270	Compute water density (RHO) from tunnel temperature, thermal expansion of manometer scales (SCALE) and manometer fluid densities (RM)
400	Read instrument zero readings before and after the run. Zero drift is accounted for by assuming a linear drift during the experiment.

580	Read run input data
	NTAP = Tunnel velocity manometer pressure tap identification
	NFLD = Manometer fluid identification
	ANGL = Angle of attack
	R = Six component strain gage dynamometer output
700-800	Correct input data for zero drift
960-1310	Non-dimensionalized forces and moments
1540-1580	Correct non-dimensional coefficients for tunnel wall effect

2. Functional Description - Dynamic Data Reduction Program

This program performs two functions:

(a) Obtains the dynamic response of the strain-gage dynamometer at the test frequency;

(b) Reduces the test data using the dynamic calibration obtained in (a).

A detailed description of each segment of the program is as follows:

Lines	Function
180	Read input constants
	COIL = Calibration coil constant (lbs/ampere)
	ECAL = Voltage drop across calibrating resistor (RMS volts)
	RCAL = Calibration resistor value (OHMS)
	DIAM = Propeller diameter
	RPM = " RPM
	RO = Fluid mass density
	Y1,Y2 = Spanwise points of application of electromagnetic shaker
	KSTOP = Control parameter to stop calculation
200	Compute calibrator force FCAL
210	Read response of dynamometer channels FA and BX to the calibrator force applied at the two spanwise points of application (index I=1 or 2). These are supplied in the form of an amplitude (J=1) and a phase (J=2).
250-310	Convert input FZ and BX amplitude/phase representation to real/imaginary representation (FZMAG,BXMAG). The latter are then converted to FORTRAN complex variables CFZ, CBX.

320-380	Compute dynamic influence coefficient matrix CA-CD using built-in FORTRAN complex arithmetic
560	Force coefficient normalizing factor $\rho n^2 D^4$
620	Read amplitude and phase of dynamometer output during test
650-700	Convert to complex variables CRUNFZ, CRUMBX as in lines 250-310
740-850	Convert input to forces by applying dynamic calibration values, non-dimensionalize and convert from complex to amplitude/phase representation
920-940	Write results and transfer to 210 for next set of test data

```
00010 C     STEADY STATE DATA REDUCTION PROGRAM
00020       INTEGER RS,S,BLANK
00030       REAL MX,MY,MZ,LIFT,MAC
00040       DIMENSION IDENT(18),ZM(2),ZI(7,2),ZF(2),NTAP(40),NFLD(40),ANOM(40)
00050      1,ANGL(40),R(40,7),DZI(7),CL(40),CD(40),CM(40),CPL(40),CY(40),
00060      2VC(5),VE(5),FM(2),C(7),CLD(40),CLSQ(40),RN(40),SI(4),CO(40)
00070      3,RHS(4),ANGD(40)
00080       DATA KI/5/,KO/6/
00090 C     VC AND VE ARE CONSTANTS RELATED WITH THE CONVERSION OF THE
00100 C     MANOMETER READING INTO WATER SPEED. WHICH OF THE 5 VALUES
00110 C     GIVEN SHOULD BE USED IS DETERMINED BY THE CHOICE OF THE
00120 C     PRESSURE TAPS AT WHICH PRESSURE WAS MEASURED
00130       DATA VC/4.11447,2.60088,0.9016,0.6214,4.7381/,VE/.49353,.5,.4724,0
00140      1.50638,.5/
00150       READ (KI,*)TWIST,SHAFT
00160  104  FORMAT(6F8.5,2F12.5)
00170       READ (KI,*) NRT,NTT,AREA,SPAN,MAC,AZL,VELINC
00180  100  FORMAT(I4,I4,F9.2,F8.3,F9.4,F8.2,F9.4)
00190       IF(AREA.LE.0) GO TO 99
00200 C     RHO CORRECTS THE VALUE OF THE TUNNEL WATER DENSITY FOR CHANGES
00210 C     IN TUNNEL TEMPERATURE.FM AND SCALE TAKE CARE OF THE EXPANSION OF
00220 C     THE FLUID AND THE MANOMETER SCALE RESPECTIVELY, DUE TO CHANGES IN
00230 C     THE ROOM TEMPERATURE.
00240       RHO=1.9574-0.00028*NTT
00250       SCALE=1.000952-13.3E-6*NRT
00260       FM(1)=1.4875-.00071*NRT
00270       FM(2)=24.5054-.00236*NRT
00280       WRITE (KO,200)
00290  200  FORMAT ('1',//17X,'RUDDER INPUT DATA'//2X,
00300      1'TR',2X,'TT',4X,'AREA',4X,'SPAN',5X,'MAC',5X,'AZL',3X,'VELINC')
00310       WRITE(KO,150)NRT,NTT,AREA,SPAN,MAC,AZL,VELINC
00320  150  FORMAT(I4,I4,F9.2,F8.3,F8.4,F8.2,F8.4)
00330   30  READ (KI,103)(IDENT(N),N=1,18)
00340  103  FORMAT (18A4)
00350 C     AT THIS POINT THE MANOMETER AND STRAIN GAUGES 'ZERO READINGS',
00360 C     (ZM AND ZI RESPECTIVELY),BEFORE AND AFTER A RUN ARE READ.IN THE
00370 C     SUBSEQUENT STEPS THE PROGRAM DECIDES THE DEGREE TO WHICH THE DIF-
00380 C     FERENCE BETWEEN THE 'ZEROES' BEFORE AND AFTER A RUN, SHOULD AFFECT
00390 C     THE READINGS TAKEN DURING THIS RUN.
00400       READ(KI,*)(ZM(K),(ZI(M,K),M=1,6),K=1,2)
00410  101  FORMAT(F5.0,10X,6(2X,F5.0))
00420       WRITE (KO,600)(IDENT(N),N=1,18)
00430  600  FORMAT(//,1X,18A4//)
00440       WRITE(KO,201)
00450  201  FORMAT(/,'  ZERO READINGS BEFORE AND AFTER'/' MAN   FX      FZ
00460      1BX      BZ      FY      BZ')
00470       WRITE(KO,204)(ZM(K),(ZI(M,K),M=1,6),K=1,2)
00480  204  FORMAT(2(F4.0,6(2X,F5.0)/))
00490       WRITE(KO,212)TWIST,SHAFT
00500   212 FORMAT ('      TWIST=',F7.1,'     SHAFT DIA.=',F7.2,'  IN.')
```

Table I.: Rudder steady state data reduction program

```
00510       DO 2 J=1,40
00520       JT=J-1
00530       JJ=J
00540 C     NTAP AND NFLD ARE THE CODE NUMBERS OF THE TAP AND FLUID CHOSEN
00550 C     ANOM(J) IS THE MANOMETER READING AT SOME ANGLE OF ATTACK DENOTED
00560 C     BY THE INDEX J. R(J,M) ARE THE OUTPUTS OF THE STRAIN GAUGES AT
00570 C     THE SAME ANGLE.
00580       READ(KI,*)NTAP(J),NFLD(J),ANOM(J),ANGL(J),(R(J,M),M=1,6)
00590  102  FORMAT(I4,I1,F5.0,F7.2,2X,F8.2,F8.2,F8.2,F8.2,F8.2,F8.2)
00600       IF(ANOM(J).LE.0.0) GO TO 3
00610    2  CONTINUE
00620  203  FORMAT(1X,I2,I1,F7.0,F5.1,2X,F6.0,3X,F6.0,3X,F6.0,3X,F6.0,3X,F6.0,
00630      13X,F6.0)
00640       GO TO 99
00650  3    WRITE(KO,202)
00660  202  FORMAT( /'    INPUT DATA AS RECORDED'/'  TF  ANOM  ANGLE     FX
00670      1    FZ       BX        BZ        FY        BY    ')
00680       WRITE(KO,203)(NTAP(J),NFLD(J),ANOM(J),ANGL(J),(R(J,M),M=1,6),J=1,J
00690      1J)
00700       BUG=1.0/(JT-1)
00710       DZM=(ZM(2)-ZM(1))*BUG
00720       DO 4 M=1,6
00730  4    DZI(M)=(ZI(M,2)-ZI(M,1))*BUG
00740       DO 7 J=1,JT
00750       IF(J.EQ.1) GO TO 6
00760       IF(NTAP(J).EQ.0) NTAP(J)=NTAP(J-1)
00770       IF(NFLD(J).EQ.0) NFLD(J)=NFLD(J-1)
00780  6    BUG=J-1
00790       ANOM(J)=ANOM(J)-ZM(1)-BUG*DZM
00800       ANGL(J)=ANGL(J)-AZL
00810       DO 7 M=1,6
00820       R(J,M)=R(J,M)-ZI(M,1)-BUG*DZI(M)
00830  7    CONTINUE
00840       WRITE(KO,205)(IDENT(N),N=1,18)
00850   205 FORMAT(///,1X,18A4//)
00860       WRITE(KO,705)(NTAP(J),NFLD(J),ANOM(J),ANGL(J),(R(J,M),M=1,6),J=1,J
00870      1T)
00880   705 FORMAT('       INPUT DATA CORRECTED FOR ZERO READINGS       '/(I3,
00890      1I1,F6.0,F7.2,2X,6F9.2))
00900  33   WRITE (KO,207)(IDENT(N),N=1,18)
00910   207 FORMAT(///,1X,18A4//)
00920   607 WRITE(KO,707)
00930   707 FORMAT('   **    RUDDER DATA REDUCTION    **'//'   ALPHA     FX-LB
00940      1    FZ-LB  BX-INLB  BZ-INLB  DRAG-LB  LIFT-LB   VER-LB  MX-INLB  M
00950      2Z-INLB  MY-INLB VEL-FPS')
00960       BEAR=MAC/(12*3.9739*EXP(67.6832/NTT))
00970       DO 9 J=1,JT
00980       I=NTAP(J)
00990       IF(I.LT.1.OR.I.GT.5) GO TO 99
01000       K=NFLD(J)
```

Table II (con't)

```
01010       IF(K.LT.1.OR.K.GT.2) GO TO 99
01020       BUG=VE(I)
01030 C     THE WATER SPEED IS COMPUTED AT THIS POINT FROM THE KNOWLEDGE
01040 C     OF THE VARIOUS CONSTANTS RELATED TO THE MANOMETER FLUID AND
01050 C     THE FACTOR CORRECTING FOR THE INTRODUCTION OF THE SPLITTER
01060 C     PLATE IN THE FLOW (VELINC).
01070       V=(ANOM(J)*FM(K)*SCALE/(VC(I)*RHO))**BUG*(1.0+VELINC)
01080 C     AT THIS POINT THE PROGRAM MAKES USE OF THE STATIC CALIBRATION
01090 C     RESULTS TO CONVERT THE FORCES INTO LBS. AND THE MOMENTS INTO
01100 C     IN-LBS TAKING ALSO CARE OF THE CROSS-TALK BETWEEN THE DIFFERENT
01110 C     GAUGES.
01120       FX=-0.076768795*R(J,1)-0.063365711*R(J,4)
01130       FZ=0.072369465*R(J,2)+0.137756*R(J,3)
01140       BX=-0.051182352*R(J,2)+0.455205523*R(J,3)
01150       BZ=-0.042513862*R(J,1)+0.22310536*R(J,4)
01160       FY=0.0
01170       BY=-0.64935*R(J,6)
01180       RAT=(ANGL(J)+AZL)*0.0174532
01190       SI(J)=SIN(RAT)
01200       CO(J)=COS(RAT)
01210 C     HERE THE LOADS MEASURED ARE RESOLVED IN THE LIFT AND DRAG DIREC-
01220 C     TIONS. THE TUNNEL WALL INTERFERENCE CORRECTION HAS NOT YET BEEN
01230 C     MADE.
01240       LIFT=FZ*CO(J)-FX*SI(J)
01250       DRAG=FX*CO(J)+FZ*SI(J)
01260       MX=BX*CO(J)+BZ*SI(J)
01270       MZ=BZ*CO(J)-BX*SI(J)
01280       VER=FY
01290       MY=BY
01300       ANGD(J)=ANGL(J)+MY/TWIST
01310       WRITE(KO,206)ANGD(J),FX,FZ,BX,BZ,DRAG,LIFT,VER,MX,MZ,MY,V
01320   206 FORMAT(11F9.2,F8.2)
01330       RVS=0.5*RHO*AREA*V**2/144.0
01340 C     HERE THE DIFFERENT FORCES AND MOMENTS ARE NON-DIMENSIONALIZED
01350       CL(J)=LIFT/RVS
01360       CLSQ(J)=CL(J)**2
01370       CD(J)=DRAG/RVS
01380       CLD(J)=CL(J)/CD(J)
01390       CM(J)=MY/RVS/MAC
01400       CPL(J)=(MX/LIFT)/SPAN
01410       CY(J)=VER/RVS
01420   9   RN(J)=V*BEAR
01430       WRITE (KO,208)(IDENT(N),N=1,18)
01440   208 FORMAT(///,1X,18A4//)
01450   608 WRITE(KO,708)
01460   708 FORMAT('   **RUDDER DATA IN NON-DIMENSIONAL FORM**'//'   ALPHA
01470      2CL      CD      CM      CPL     CY      L/D     RN*10**-6    CLSQ')
01480       WRITE(KO,209)(ANGD(J),CL(J),CD(J),CM(J),CPL(J),CY(J),CLD(J),RN(J),
01490      1CLSQ(J),J=1,JT)
01500   209 FORMAT(F8.2,F7.3,2F8.4,3F7.3,F8.3,5X,F7.4)
```

Table II (con't)

```
01510        DO 15 J=1,JT
01520 C      HERE THE RUDDER ANGLE AND THE DRAG COEFFICIENT ARE BOTH
01530 C      CORRECTED FOR TUNNEL WALL INTERFERENCE.
01540        ANGD(J)=ANGD(J)+0.02045*AREA*CL(J)
01550        CD(J)=CD(J)+0.0003570*AREA*CL(J)**2
01560  15    CLD(J)=CL(J)/CD(J)
01570        WRITE(KO,211) (IDENT(N),N=1,18)
01580   211 FORMAT(///,1X,18A4//)
01590   611 WRITE(KO,711)
01600   711 FORMAT('      PRIOR DATA CORRECTED FOR TUNNEL INTERFERENCE'//'   AL
01610      1PHA     CL      CD      CM      CPL     CY      L/D     RN*10**-6    CLSQ
01620      2')
01630        WRITE(KO,209)(ANGD(J),CL(J),CD(J),CM(J),CPL(J),CY(J),CLD(J),RN(J),
01640      1CLSQ(J),J=1,JT)
01650        GO TO 30
01660  99    STOP
01670        END
```

Table II (con't)

RUDDER INPUT DATA

TR	TT	AREA	SPAN	MAC	AZL	VELINC
82	85	74.19	9.354	7.9670	0.0	0.0910

THE FOLLOWING RESULTS ARE FOR A CLEARANCE RATIO OF .37

ZERO READINGS BEFORE AND AFTER

MAN	FX	FZ	BX	BZ	FY	BZ
0.	0.	500.	-650.	0.	0.	0.
0.	-30.	494.	-648.	-4.	0.	0.

TWIST=10000.0 SHAFT DIA.= 2.00 IN.

INPUT DATA AS RECORDED

TF	ANON	ANGLE	FX	FZ	BX	BZ	FY	BY
11	1506.	0.0	-16.	622.	-666.	-68.	0.	-38.
00	1506.	5.0	-19.	99.	-24.	-67.	0.	-70.
00	1506.	10.0	-65.	-440.	632.	36.	0.	-38.
00	1503.	15.0	-154.	-978.	1318.	258.	0.	-102.
00	1506.	20.0	-286.	-1504.	1964.	590.	0.	-96.
00	971.	25.0	-278.	-1158.	1476.	676.	0.	-52.
00	971.	30.0	-444.	-1472.	1356.	1020.	0.	-20.
00	-100.	0.0	0.	0.	0.	0.	0.	0.

THE FOLLOWING RESULTS ARE FOR A CLEARANCE RATIO OF .37

INPUT DATA CORRECTED FOR ZERO READINGS

11	1506.	0.0	-16.00	122.00	-16.00	-68.00	0.0	-38.00
11	1506.	5.00	-13.00	-499.00	625.67	-66.33	0.0	-70.00
11	1506.	10.00	-53.00	-938.00	1281.33	37.33	0.0	-38.00
11	1506.	15.00	-136.00	-1475.00	1967.00	260.00	0.0	-102.00
11	1506.	20.00	-262.00	-2000.00	2612.67	592.67	0.0	-96.00
11	971.	25.00	-248.00	-1653.00	21[illegible]	[illegible]7.33	0.	-52.00
11	971.	30.00	-408.00	-1966.00	2504.00	1024.00	0.0	-20.00

Table III: Sample output of rudder steady state data reduction program

THE FOLLOWING RESULTS ARE FOR A CLEARANCE RATIO OF .37

** RUDDER DATA REDUCTION **

ALPHA	FX-LB	FZ-LB	BX-INLB	BZ-INLB	DRAG-LB	LIFT-LB	VER-LB	MX-INLB	MZ-INLB	MY-INLB	VEL-FPS
0.00	5.54	6.62	-13.53	-14.49	5.54	6.62	0.0	-13.53	-14.49	24.68	17.31
5.00	5.20	56.59	305.74	-14.25	10.11	55.92	0.0	303.33	-40.84	45.45	17.31
10.00	1.70	108.63	631.28	10.58	20.54	106.68	0.0	623.53	-99.20	24.68	17.31
15.01	-6.33	164.22	970.88	63.79	36.67	160.19	0.0	954.31	-189.67	66.23	17.31
20.01	-17.44	215.17	1281.66	143.37	57.20	208.16	0.0	1262.80	-307.05	62.34	17.31
25.00	-24.01	175.61	1051.61	162.11	51.36	166.95	0.0	1021.59	-297.51	33.77	13.94
30.00	-33.56	202.60	1240.46	245.81	72.28	192.29	0.0	1197.17	-407.35	12.99	13.94

THE FOLLOWING RESULTS ARE FOR A CLEARANCE RATIO OF .37

RUDDER DATA IN NON-DIMENSIONAL FORM

ALPHA	CL	CD	CM	CPL	CY	L/D	RN*10**-6	CLSQ
0.00	0.044	0.0371	0.0208	-0.218	0.0	1.196	1.304	0.0020
5.00	0.375	0.0678	0.0382	0.580	0.0	5.529	1.304	0.1405
10.00	0.715	0.1377	0.0208	0.625	0.0	5.194	1.304	0.5114
15.01	1.074	0.2458	0.0557	0.637	0.0	4.368	1.304	1.1531
20.01	1.395	0.3835	0.0525	0.649	0.0	3.639	1.304	1.9472
25.00	1.726	0.5310	0.0438	0.654	0.0	3.251	1.050	2.9789
30.00	1.988	0.7471	0.0169	0.666	0.0	2.661	1.050	3.9520

THE FOLLOWING RESULTS ARE FOR A CLEARANCE RATIO OF .37

PRIOR DATA CORRECTED FOR TUNNEL INTERFERENCE

ALPHA	CL	CD	CM	CPL	CY	L/D	RN*10**-6	CLSQ
0.07	0.044	0.0372	0.0208	-0.218	0.0	1.195	1.304	0.0020
5.57	0.375	0.0715	0.0332	0.580	0.0	5.242	1.304	0.1405
11.09	0.715	0.1512	0.0208	0.625	0.0	4.729	1.304	0.5114
16.64	1.074	0.2764	0.0557	0.637	0.0	3.885	1.304	1.1531
22.12	1.395	0.4350	0.052.	0.649	0.0	3.208	1.304	1.9472
27.62	1.726	0.6009	0.0438	0.654	0.0	2.830	1.050	2.9789
33.02	1.988	0.8517	0.0169	0.666	0.0	2.334	1.050	3.9520

Table III (con't)

THE FOLLOWING RESULTS ARE FOR A CLEARANCE RATIO OF.37

ZERO READINGS BEFORE AND AFTER

MAN	FX	FZ	BX	BZ	FY	BZ
0.	0.	-506.	630.	0.	0.	0.
0.	-28.	-482.	630.	4.	0.	0.

TWIST=10000.0 SHAFT DIA.= 2.00 IN.

INPUT DATA AS RECORDED

TF	ANOM	ANGLE	FX	FZ	BY	BZ	FY	BY
11	1506.	0.0	-3.	-400.	616.	-72.	0.	-37.
00	1506.	-5.0	-26.	126.	6.	18.	0.	-6.
00	1506.	-10.0	-84.	698.	-634.	204.	0.	12.
00	1506.	-15.0	-156.	1312.	-1320.	464.	0.	12.
00	1506.	-20.0	-210.	1998.	-2020.	714.	0.	-2.
00	971.	-25.0	-226.	1492.	-1492.	724.	0.	-24.
00	971.	-30.0	-234.	2035.	-2032.	870.	0.	-60.
00	-100.	0.0	0.	0.	0.	0.	0.	0.

THE FOLLOWING RESULTS ARE FOR A CLEARANCE RATIO OF.37

INPUT DATA CORRECTED FOR ZERO READINGS

11	1506.	0.0	-3.00	106.00	-14.00	-72.00	0.0	-37.00
11	1506.	-5.00	-21.33	628.00	-624.00	17.33	0.0	-6.00
11	1506.	-10.00	-74.67	1190.00	-1264.00	202.67	0.0	12.00
11	1506.	-15.00	-142.00	1806.00	-1950.00	462.00	0.0	12.00
11	1506.	-20.00	-191.33	2488.00	-2650.00	711.33	0.0	-2.00
11	971.	-25.00	-202.67	1978.00	-2122.00	720.67	0.0	-24.00
11	971.	-30.00	-206.00	2517.00	-2662.00	866.00	0.0	-60.00

Table III (con't)

THE FOLLOWING RESULTS ARE FOR A CLEARANCE RATIO OF.37

** RUDDER DATA REDUCTION **

ALPHA	FX-LB	FZ-LB	BX-INLB	BZ-INLB	DRAG-LB	LIFT-LB	VEB-LB	MX-INLB	MZ-INLB	MY-INLB	VEL-FPS
0.00	4.79	5.74	-11.80	-15.94	4.79	5.74	0.0	-11.80	-15.94	24.03	17.31
-5.00	0.54	-40.51	-316.19	4.77	4.07	-40.31	0.0	-315.40	-22.80	3.90	17.31
-10.00	-7.11	-87.57	-636.59	48.39	8.20	-87.47	0.0	-635.32	-62.89	-7.79	17.31
-15.00	-18.37	-137.92	-980.09	109.11	17.95	-137.98	0.0	-974.93	-148.27	-7.79	17.31
-20.00	-30.39	-185.00	-1333.64	166.84	34.72	-184.23	0.0	-1310.27	-299.35	1.30	17.31
-25.00	-30.11	-149.17	-1067.18	169.40	35.76	-147.92	0.0	-1038.79	-297.48	15.58	13.94
-30.00	-39.06	-184.55	-1340.58	201.97	58.45	-179.36	0.0	-1261.96	-495.36	38.96	13.94

THE FOLLOWING RESULTS ARE FOR A CLEARANCE RATIO OF.37

RUDDER DATA IN NON-DIMENSIONAL FORM

ALPHA	CL	CD	CM	CPL	CY	L/D	RN*10**-6	CLSQ
0.00	0.038	0.0321	0.0202	-0.220	0.0	1.198	1.304	0.0015
-5.00	-0.270	0.0273	0.0033	0.836	0.0	-9.909	1.304	0.0730
-10.00	-0.586	0.0550	-0.0066	0.776	0.0	-10.662	1.304	0.3438
-15.00	-0.925	0.1203	-0.0066	0.755	0.0	-7.687	1.304	0.8555
-20.00	-1.235	0.2327	0.0011	0.760	0.0	-5.306	1.304	1.5253
-25.00	-1.529	0.3696	0.0202	0.751	0.0	-4.137	1.050	2.3385
-30.00	-1.854	0.6042	0.0506	0.752	0.0	-3.069	1.050	3.4381

THE FOLLOWING RESULTS ARE FOR A CLEARANCE RATIO OF.37

PRIOR DATA CORRECTED FOR TUNNEL INTERFERENCE

ALPHA	CL	CD	CM	CPL	CY	L/D	RN*10**-6	CLSQ
0.06	0.038	0.0322	0.0202	-0.220	0.0	1.197	1.304	0.0015
-5.41	-0.270	0.0292	0.0033	0.836	0.0	-9.253	1.304	0.0730
-10.89	-0.586	0.0641	-0.0066	0.776	0.0	-9.147	1.304	0.3438
-16.40	-0.925	0.1430	-0.0066	0.755	0.0	-6.469	1.304	0.8555
-21.87	-1.235	0.2731	0.0011	0.760	0.0	-4.522	1.304	1.5253
-27.32	-1.529	0.4316	0.0202	0.751	0.0	-3.543	1.050	2.3385
-32.81	-1.854	0.6953	0.0506	0.752	0.0	-2.667	1.050	3.4381

Table III (con't)

```
00010 C     DYNAMIC DATA REDUCTION PROGRAM
00020 C     THE FIRST PART OF THIS PROGRAM IS USED TO CALIBRATE THE
00030 C     TWO DYNAMOMETER CHANNELS WE ARE EXAMINING.A KNOWN FORCE 'FCAL',
00040 C     IS APPLIED AND THE RESPONSE OF EACH CHANNEL TO THIS FORCE,'FZ',
00050 C     AND 'BX' RESPECTIVELY, IS COMPUTED AT TWO DIFFERENT LOCATIONS
00060 C     OF THE APPLIED FORCE.THESE RESULTS CAN BE COMBINED TO GIVE AN
00070 C     INFLUENCE COEFFICIENT MATRIX CONTAINING THE ELEMENTS 'CA','CB',
00080 C     'CC','CD',WHICH ARE USED LATER ON DURING THE EXPERIMENT TO
00090 C     EVALUATE THE AMPLITUDE AND PHASE ANGLE OF THE TWO RESPONSES,
00100 C     AS INDICATED IN THE SECOND PART OF THE PROGRAM.
00110       COMPLEX CFZ(2),CBX(2),CRUNFZ,CRUNBX,CA,CB,CC,CD,CFORCE,CMPLX,CMPRN
00120      1T,CDENOM
00130       DIMENSION FZ(2,2),BX(2,2),FZMAG(2,2),BXMAG(2,2),RUNBX(2),RUNFZ(2)
00140      1,RFZ(2),RBX(2),LABEL(18)
00150       DATA KI/5/,KO/6/
00160       WRITE(6,60)
00170 60    FORMAT(1X,'EXECUTION BEGINS'//)
00180 1     READ (KI,*)COIL,ECAL,RCAL,DIAM,RPM,RO,Y1,Y2,KSTOP
00190       IF (KSTOP.EQ.0) GO TO 50
00200       FCAL=COIL*ECAL*1.414214/RCAL
00210       READ(KI,*) ((FZ(I,J),J=1,2),I=1,2),((BX(I,J),J=1,2),I=1,2)
00220 C     NEXT THE PROGRAM READS THE CALIBRATION VALUES. THE FIRST INDEX
00230 C     REFERS TO LOCATION ON THE RUDDER AND THE SECOND IF 1 IS THE AMPLI-
00240 C     TUDE OF THE SIGNAL AND IF 2,IS THE PHASE.
00250       DO 15 K=1,2
00260       FZMAG(K,1)=FZ(K,1)*COS(0.01745329*FZ(K,2))
00270       BXMAG(K,1)=BX(K,1)*COS(0.01745329*BX(K,2))
00280       FZMAG(K,2)=FZ(K,1)*SIN(0.01745329*FZ(K,2))
00290       BXMAG(K,2)=BX(K,1)*SIN(0.01745329*BX(K,2))
00300       CFZ(K)=CMPLX(FZMAG(K,1),FZMAG(K,2))
00310 15    CBX(K)=CMPLX(BXMAG(K,1),BXMAG(K,2))
00320       CDENOM=CBX(1)*CFZ(2)-CBX(2)*CFZ(1)
00330 C     AT THIS POINT THE PROGRAM HAS REWRITTEN THE INPUT READINGS IN
00340 C     COMPLEX FORM AND IS READY TO COMPUTE THE INFLUENCE COEFFICIENTS
00350       CA=((CBX(1)-CBX(2))/CDENOM)*FCAL
00360       CB=((CFZ(2)-CFZ(1))/CDENOM)*FCAL
00370       CC=((CBX(2)*Y2-CBX(2)*Y1)/CDENOM)*FCAL
00380       CD=((CFZ(2)*Y1-CFZ(1)*Y2)/CDENOM)*FCAL
00390       WRITE (KO,20) COIL,ECAL,RCAL,DIAM,RPM,RO,Y1,Y2,FCAL
00400 20    FORMAT('1',4X,'COIL=',F5.3,1X,'(LB/AMP)',/,5X,'ECAL=',F5.3,1
00410      1X,'(VOLTS)',/,5X,'RCAL=',F5.3,1X,'(OHMS)',/,5X,'PROP.DIAM='
00420      2,F6.3,1X,'(IN)',/,5X,'RPM=',F6.1,/,5X,'DENSITY=',F10.5,1X,
00430      3'(LBS/FT**3)',/,5X,'L1=',F5.3,1X,'(IN)',/,5X,'L2=',F5.3,1X,
00440      4'(IN)',///,5X,'CALIBRATION FORCE=',F10.5,1X,'(LBS)')
00450 21    FORMAT(///,28X,'CALIBRATION READINGS',///,25X,'AMPL',8X,'PHASE',
00460      113X,'AMPL',8X,'PHASE',//,2X,'FORCE AT L1',2X,'FZREAD=',F
00470      210.5,4X,F8.4,2X,'BXREAD=',F10.5,4X,F8.4,/,2X,'FORCE AT L2',
00480      32X,'FZREAD=',F10.5,4X,F8.4,2X,'BXREAD=',F10.5,4X,F8.4/)
00490 25    WRITE(KO,21) (FZ(I,1),FZ(I,2),BX(I,1),BX(I,2),I=1,2)
00500       WRITE(KO,22) (FZMAG(I,1),FZMAG(I,2),BXMAG(I,1),BXMAG(I,2)
```

Table IV: Rudder dynamic data reduction program

```
00510       1,I=1,2)
00520 22     FORMAT(///,1X,'AT L1',3X,'REALFZ=',F10.5,1X,'IMAGFZ=',F10.5,
00530       11X,'REALBX=',F10.5,1X,'IMAGBX=',F10.5,//,1X,'AT L2',3X,
00540       2'REALFZ=',F10.5,1X,'IMAGFZ=',F10.5,1X,'REALBX=',F10.5,1X,
00550       3'IMAGBX=',F10.5/)
00560        BUG=12.0**4/(RO*((RPM/60.0)**2)*(DIAM**4))
00570 2      READ(KI,40) (LABEL(N),N=1,18)
00580 40     FORMAT(18A4)
00590 C      AT THIS POINT THE PROGRAM READS THE VALUES OF THE LOADS MEASURED
00600 C      IN THE ACTUAL EXPERIMENT. THE INDEX AS BEFORE DIFFERENTIATES
00610 C      BETWEEN AMPLITUDE AND PHASE.
00620        READ(KI,*) RFZ(1),RFZ(2),RBX(1),RBX(2),NCODE
00630 42     FORMAT(4F10.5,I10)
00640        IF (NCODE.EQ.0) GO TO 1
00650        RUNBX(1)=RBX(1)*COS(0.01745329*RBX(2))
00660        RUNBX(2)=RBX(1)*SIN(0.01745329*RBX(2))
00670        RUNFZ(1)=RFZ(1)*COS(0.01745329*RFZ(2))
00680        RUNFZ(2)=RFZ(1)*SIN(0.01745329*RFZ(2))
00690        CRUNFZ=CMPLX(RUNFZ(1),RUNFZ(2))
00700        CRUNBX=CMPLX(RUNBX(1),RUNBX(2))
00710 C      CFORCE AND CMOMNT ARE THE FORCE AND MOMENT VALUES OF THE READINGS
00720 C      CORRECTED FOR THE CROSS TALK BETWEEN THE TWO GAUGES. THEY ARE IN
00730 C      COMPLEX FORM AND THEIR AMPLITUDES ARE IN LBS.
00740        CFORCE=CRUNFZ*CA+CRUNBX*CB
00750        CMOMNT=CRUNFZ*CC+CRUNBX*CD
00760        FREAL=REAL(CFORCE)
00770        FIMAG=AIMAG(CFORCE)
00780        BREAL=REAL(CMOMNT)
00790        BIMAG=AIMAG(CMOMNT)
00800 C      FAMP AND BAMP ARE THE FORCE AND MOMENT AMPLITUDES IN NON-DIMENSIO-
00810 C      NAL FORM. THEY CORRESPOND TO 'KF*1000' AND 'KB*1000' ON THE GRAPHS
00820        FAMP=SQRT(FREAL**2+FIMAG**2)*BUG*1000.0
00830        BAMP=SQRT(BREAL**2+BIMAG**2)*BUG*1000.0/DIAM
00840        FPHASE=ATAN(FIMAG/FREAL)*57.2958
00850        BPHASE=ATAN(BIMAG/BREAL)*57.2958
00860 46     FORMAT(//,1X,18A4,//,28X,'EXPERIMENT READINGS',///,20X,'AMPL',
00870       16X,'PHASE',23X,'AMPL',6X,'PHASE',//,5X,'RFZ',7X,F10.5,3X,
00880       2F8.4,7X,'RBX',7X,F10.5,3X,F8.4,//,5X,'FREAL=',F10.5,//,
00890       35X,'FIMAG=',F10.5,//,5X,'BREAL=',F10.5,//,5X,'BIMAG=',F10.5,/
00900       4/,5X,'FAMP*1000=',F10.5,9X,'FPHASE=',F10.5,//,5X,'BAMP*1000='
00910       5,F10.5,9X,'BPHASE=',F10.5)
00920        WRITE(KO,46)(LABEL(N),N=1,18),RFZ(1),RFZ(2),RBX(1),RBX(2),
00930       1FREAL,FIMAG,BREAL,BIMAG,FAMP,FPHASE,BAMP,BPHASE
00940        GO TO 2
00950 50     WRITE(KO,55)
00960 55     FORMAT ('1')
00970        STOP
00980        END
```

Table IV (con't)

COIL=0.750 (LB/AMP)
ECAL=4.000 (VOLTS)
RCAL=4.600 (OHMS)
PROP.DIAM= 9.846 (IN)
RPM=1500.0
DENSITY= 1.93780 (SLUGS/FT**3)
L1=3.000 (IN)
L2=9.000 (IN)

CALIBRATION FORCE= 0.92231 (LBS)

CALIBRATION READINGS

		AMPL	PHASE		AMPL	PHASE
FORCE AT L1	FZREAD=	0.28503	117.0000	BXREAD=	0.12500	270.0000
FORCE AT L2	FZREAD=	0.06000	90.0000	BXREAD=	0.60000	270.0000

AT L1	REALFZ=	-0.09307	IMAGFZ=	0.18266	REALBX=	-0.00000	IMAGBX=	-0.12500
AT L2	REALFZ=	0.00000	IMAGFZ=	0.06000	REALBX=	-0.00000	IMAGBX=	-0.60000

Table V: Sample output of dynamic data reduction program

RUDDER AT 1 INCH OFF CENTRELINE (DESIGN POSITION). CLEARANCE RATIO .33

EXPERIMENT READINGS

	AMPL	PHASE		AMPL	PHASE
RFZ	0.32000	284.0000	RBX	0.65000	36.0000

FREAL= -1.72153

FIMAG= 0.87087

BREAL= -6.89750

BIMAG= 7.36398

FAMP*1000= 3.51471 FPHASE= -26.83350

BAMP*1000= 1.86689 BPHASE= -46.87341

RUDDER AT 1 INCH OFF CENTRELINE (DESIGN POSITION). CLEARANCE RATIO .37

EXPERIMENT READINGS

	AMPL	PHASE		AMPL	PHASE
RFZ	0.38500	252.0000	RBX	1.15000	45.0000

FREAL= -2.12280

FIMAG= 1.88896

BREAL= -12.49031

BIMAG= 12.15800

FAMP*1000= 5.17670 FPHASE= -41.66414

BAMP*1000= 3.22514 BPHASE= -44.22762

Table V (con't)

RUDDER AT 1 INCH OFF CENTRELINE (DESIGN POSITION). CLEARANCE RATIO .41

EXPERIMENT READINGS

	AMPL	PHASE		AMPL	PHASE
RFZ	0.12500	288.0000	RBX	0.24000	180.0000

FREAL= -0.41909

FIMAG= -0.20247

BREAL= -0.59555

BIMAG= -3.08378

FAMP*1000= 0.84793 FPHASE= 25.78540

BAMP*1000= 0.58113 BPHASE= 79.06931

RUDDER AT 1 INCH OFF CENTRELINE (DESIGN POSITION). CLEARANCE RATIO .45

EXPERIMENT READINGS

	AMPL	PHASE		AMPL	PHASE
RFZ	0.31500	252.0000	RBX	0.95000	360.0000

FREAL= -0.98530

FIMAG= 2.00929

BREAL= -1.40015

BIMAG= 13.92307

FAMP*1000= 4.07690 FPHASE= -63.87798

BAMP*1000= 2.58915 BPHASE= -84.25746

Table V (con't)

RUDDER AT 1 INCH OFF CENTRELINE (DESIGN POSITION). CLEARANCE RATIO .49

EXPERIMENT READINGS

	AMPL	PHASE		AMPL	PHASE
RFZ	0.34500	243.0000	RBX	0.90000	18.0000

FREAL= -1.22266

FIMAG= 2.05548

BREAL= -4.97760

BIMAG= 12.89301

FAMP*1000= 4.35702 FPHASE= -59.25436

BAMP*1000= 2.55717 BPHASE= -68.88991

RUDDER AT 1 INCH OFF CENTRELINE (DESIGN POSITION). CLEARANCE RATIO .53

EXPERIMENT READINGS

	AMPL	PHASE		AMPL	PHASE
RFZ	0.45500	243.0000	RBX	1.32500	18.0000

FREAL= -1.68770

FIMAG= 2.86159

BREAL= -7.16850

BIMAG= 18.74754

FAMP*1000= 6.05233 FPHASE= -59.46878

BAMP*1000= 3.71375 BPHASE= -69.07466

Table V (con't)

RUDDER AT 1 INCH OFF CENTRELINE (DESIGN POSITION). CLEARANCE RATIO .57

EXPERIMENT READINGS

	AMPL	PHASE		AMPL	PHASE
RFZ	0.52500	252.0000	RBX	1.70000	54.0000

FREAL= -3.19651

FIMAG= 2.39540

BREAL= -20.56535

BIMAG= 15.04536

FAMP*1000= 7.27701 FPHASE= -36.84721

BAMP*1000= 4.71474 BPHASE= -36.18875

RUDDER AT 1 INCH OFF CENTRELINE (DESIGN POSITION). CLEARANCE RATIO .61

EXPERIMENT READINGS

	AMPL	PHASE		AMPL	PHASE
RFZ	0.39000	270.0000	RBX	1.35000	72.0000

FREAL= -2.91310

FIMAG= 0.97610

BREAL= -19.09775

BIMAG= 6.24727

FAMP*1000= 5.59702 FPHASE= -18.52466

BAMP*1000= 3.71787 BPHASE= -18.11400

Table V (con't)

RUDDER AT 1 INCH OFF CENTRELINE (DESIGN POSITION). CLEARANCE RATIO .65

EXPERIMENT READINGS

	AMPL	PHASE		AMPL	PHASE
RFZ	0.19500	261.0000	RBX	0.62500	99.0000

FREAL= -1.30840

FIMAG= 0.21919

BREAL= -9.05109

BIMAG= -0.82759

FAMP*1000= 2.41684 FPHASE= -9.51000

BAMP*1000= 1.68169 BPHASE= 5.22434

RUDDER AT 1 INCH OFF CENTRELINE (DESIGN POSITION). CLEARANCE RATIO .69

EXPERIMENT READINGS

	AMPL	PHASE		AMPL	PHASE
RFZ	0.12500	252.0000	RBX	0.23500	27.0000

FREAL= -0.48947

FIMAG= 0.57579

BREAL= -1.93851

BIMAG= 3.25764

FAMP*1000= 1.37676 FPHASE= -49.63249

BAMP*1000= 0.70140 BPHASE= -59.24458

Table V (con't)

RUDDER AT 1 INCH OFF CENTRELINE (DESIGN POSITION). CLEARANCE RATIO .73

EXPERIMENT READINGS

	AMPL	PHASE		AMPL	PHASE
RFZ	0.23000	225.0000	RBX	0.55000	18.0000

FREAL= -0.54299

FIMAG= 1.43159

BREAL= -2.75169

BIMAG= 8.12841

FAMP*1000= 2.78935 FPHASE= -69.22874

BAMP*1000= 1.58782 BPHASE= -71.29758

RUDDER AT 1 INCH OFF CNTRELINE (DESIGN POSITION). CLEARANCE RATIO .77

EXPERIMENT READINGS

	AMPL	PHASE		AMPL	PHASE
RFZ	0.30000	243.0000	RBX	0.73800	45.0000

FREAL= -1.36093

FIMAG= 1.46830

BREAL= -3.01360

BIMAG= 8.16617

FAMP*1000= 3.64723 FPHASE= -47.17331

BAMP*1000= 2.11696 BPHASE= -45.54025

Table V (con't)

RUDDER AT 1 INCH OFF CENTRELINE (DESIGN POSITION). CLEARANCE RATIO .81

EXPERIMENT READINGS

	AMPL	PHASE		AMPL	PHASE
RFZ	0.27000	261.0000	RBX	0.76400	81.0000

FREAL= -1.73683

FIMAG= 0.62921

BREAL= -11.25936

BIMAG= 2.28652

FAMP*1000= 3.36536 FPHASE= -19.91405

BAMP*1000= 2.12582 BPHASE= -11.47938

RUDDER AT 1 INCH OFF CENTRELINE (DESIGN POSITION). CLEARANCE RATIO .85

EXPERIMENT READINGS

	AMPL	PHASE		AMPL	PHASE
RFZ	0.18000	270.0000	RBX	0.60000	95.0000

FREAL= -1.30647

FIMAG= 0.15409

BREAL= -8.82014

BIMAG= -0.39026

FAMP*1000= 2.39661 FPHASE= -6.72673

BAMP*1000= 1.63357 BPHASE= 2.53347

Table V (con't)

RUDDER AT 1 INCH OFF CENTRELINE (DESIGN POSITION). CLEARANCE RATIO .93

EXPERIMENT READINGS

	AMPL	PHASE		AMPL	PHASE
RFZ	0.12000	252.0000	RBX	0.43800	117.0000

FREAL= -0.74505

FIMAG= 0.01817

BREAL= -5.60540

BIMAG= -2.29081

FAMP*1000= 1.35772 FPHASE= -1.39727

BAMP*1000= 1.12042 BPHASE= 22.22878

RUDDER AT 1 INCH OFF CENTRELINE (DESIGN POSITION). CLEARANCE RATIO 1.01

EXPERIMENT READINGS

	AMPL	PHASE		AMPL	PHASE
RFZ	0.20000	243.0000	RBX'	0.49000	81.0000

FREAL= -1.02251

FIMAG= 0.62692

BREAL= -7.09139

BIMAG= 1.78392

FAMP*1000= 2.18504 FPHASE= -31.51349

BAMP*1000= 1.35298 BPHASE= -14.12039

Table V (con't)

RUDDER AT 1 INCH OFF CENTRELINE (DESIGN POSITION). CLEARANCE RATIO 1.09

EXPERIMENT READINGS

	AMPL	PHASE		AMPL	PHASE
RFZ	0.23500	315.0000	RRX	0.60000	126.0000

FREAL= -1.37119

FIMAG= -0.76199

BREAL= -7.60370

BIMAG= -5.19154

FAMP*1000= 2.85781 FPHASE= 29.06151

BAMP*1000= 1.70354 BPHASE= 34.32390

Table V (con't)